JOURNAL OF GEOPHYSICAL RESEARCH, VOL. 99, NO. D10, PAGES 20,725–20,756, OCTOBER 20, 1994

Sulfate over the North Atlantic and adjacent continental regions: Evaluation for October and November 1986 using a three-dimensional model driven by observation-derived meteorology

Carmen M. Benkovitz
Environmental Chemistry Division, Brookhaven National Laboratory, Upton, New York

Carl M. Berkowitz and Richard C. Easter
Earth and Environmental Sciences Center, Pacific Northwest Laboratory, Richland, Washington

Seth Nemesure, Richard Wagener, and Stephen E. Schwartz
Environmental Chemistry Division, Brookhaven National Laboratory, Upton, New York

Abstract. A high-resolution three-dimensional Eulerian transport and transformation model has been developed to simulate concentrations of tropospheric sulfate for specific times and locations; it was applied over the North Atlantic and adjacent continental regions during October and November 1986. The model represents emissions of anthropogenic SO_2 and sulfate and of biogenic sulfur species, horizontal and vertical transport, gas phase oxidation of SO_2 and dimethylsulfide, aqueous phase oxidation of SO_2, and wet and dry deposition of SO_2, sulfate, and methanesulfonic acid (MSA). The meteorological driver is the 6-hour output from the forecast model of the European Centre for Medium-Range Weather Forecasts. Calculated sulfate concentrations and column burdens, examined in detail for specific dates, are related to existing weather patterns. These quantities exhibit rich temporal and spatial structure; the characteristic ($1/e$) autocorrelation time for the sulfate column burdens over the central North Atlantic averages 10 hours; 95% of the values are 25 hours or less. The characteristic distance of spatial autocorrelation over this region depends on direction; the minimum value of the average is 900 km and the minimum values for the 10th and 90th percentiles are 400 and 1700 km. Daily average model sulfate concentrations at the lowest vertical level accurately represent the spatial variability, episodicity, and absolute magnitudes of surface concentrations measured by monitoring stations in Europe, Canada, New York state, and Barbados; over 50% of model concentrations are within a factor of 3 of the observations. Over 50% of weekly model sulfate wet deposition amounts are within a factor of 3 of observations from U.S. monitoring stations. Over the 34-day period modeled, contributions from anthropogenic emissions to the sulfate over the mid North Atlantic Ocean ranged from 44 to 66%, contributions from biogenic emissions were between 6 and 12%. Calculated average yields for sulfate (47 to 72%) and MSA (13%), and turnover times for SO_2 (2 to 3 days) and sulfate and MSA (4 to 8 days) are comparable to previous estimates; however, these quantities depend on meteorological conditions and on the geographical and vertical distributions of the material.

1. Introduction

This paper describes a set of simulations of tropospheric sulfate concentrations and column burdens (vertical column integral of concentration) at specific times and locations, suitable for comparison with in situ and remote measurements. A key motivation for these calculations is the hypothesis that anthropogenic sulfate aerosol influences clear-sky and cloud albedo and can thus influence climate [*Twomey*, 1977; *Twomey et al.*, 1984; *Schwartz*, 1988a; *Charlson et al.*, 1990, 1991, 1992; *Wigley and Raper*, 1992; *Kiehl and Briegleb*, 1993]. The mechanisms are hypothesized to be (1) an enhancement of clear-sky albedo due to direct light scattering of solar radiation by sulfate aerosol particles resulting from emissions of SO_2 associated with fossil fuel combustion and other industrial activity, and (2) an enhancement of average cloud albedo due to increases in the number concentration of cloud condensation nuclei (CCN) and the resulting increase in the concentration of cloud droplets. Albedo changes influence the global energy budget; the magnitude of this influence is estimated to be comparable, but of opposite sign, to current global forcing by anthropogenic enhancement of greenhouse gases [*Charlson et al.*, 1991, 1992; *Wigley and Raper*, 1992; *Kiehl and Briegleb*, 1993].

Copyright 1994 by the American Geophysical Union.

Paper number 94JD01634.
0148-0227/94/94JD-01634$05.00

Previous attempts to identify correlations of satellite observations of albedo with regions influenced by anthropogenic SO_2 emissions have yielded mixed results. *Kim and Cess* [1993], examining monthly averaged low-level marine cloud albedo obtained from the Earth Radiation Budget Experiment (ERBE) over all oceans of the world, detected cloud albedo enhancement over coastal areas affected by anthropogenic SO_2 emissions but not over ocean areas well removed from source regions. *Falkowski et al.* [1992] found that the monthly averaged albedo of low-level marine stratus clouds over the North Atlantic Ocean obtained from ERBE exhibited correlation with ocean productivity inferred from the coastal zone color scanner (CZCS) chlorophyll concentrations, and concluded that much of the variability in cloud albedo could be accounted for by biogenic emissions of sulfate precursors. *Han et al.* [1994] conducted a near-global survey based on satellite data from the International Satellite Cloud Climatology Project and found evidence of a systematic interhemispheric difference in the average cloud droplet radii for both marine and continental clouds (average radius was smaller in the northern hemisphere), consistent with possible influence by anthropogenic CCN in the northern hemisphere. All these studies were based on monthly or annual data averaged over regions with extent of several thousand kilometers. However, sulfate concentrations and aerosol optical depth are highly variable, with space and time scales of about a day and a few hundred kilometers [*Wesely*, 1982; *Schaug et al.*, 1988, 1989; *Husain and Dutkiewicz*, 1990]. Therefore, examination of the correlations between sulfate aerosol loadings and clear-sky and cloud albedo at these geographical and temporal scales appears to be necessary to better discern the influences of both anthropogenic and biogenic sulfur on albedo.

In order to examine such correlations it is necessary to obtain sulfate aerosol concentration data at times and locations coincident with the satellite observations. Atmospheric measurements of sulfate aerosol concentrations are available from ground level monitoring networks [*Schaug et al.*, 1988; *U.S. Environmental Protection Agency (EPA)*, 1988, 1989]; however, coverage provided by these networks is limited to a few regions and is at best daily in time. Therefore, estimates of regional and global sulfate aerosol loading, and the contributions to this loading from different sources, can be obtained only by the use of models.

Several hemispheric- and global-scale transport and transformation models have been used to study atmospheric distributions of SO_2 and sulfate. *Rodhe and Isaksen* [1980] conducted simulations for January and July using a two-dimensional (height-latitude) global model driven by climatological data. *Langner and Rodhe* [1991] used a global-scale model with 10° horizontal grid spacing, climatological monthly mean winds, and statistically derived values for cloud cover and precipitation. *Erickson et al.* [1991] computed global distributions of CCN from sulfur emissions using a regional- to global-scale Lagrangian parcel model [*Walton et al.*, 1988], with 330-km horizontal grid spacing and approximately 50,000 constant-mass air parcels, driven by meteorological fields from a general circulation model (GCM). *Giorgi and Chameides* [1986] used a GCM with 4.5° × 7.5° horizontal grid spacing and rainout parameterization to estimate average rainout lifetimes of highly soluble particulate and gaseous atmospheric compounds, and showed that their results are in agreement with estimates inferred from observations when these are classified according to the height of release of the measured species. *Balkanski et al.* [1993] used an Eulerian global model with 4° × 5° horizontal grid spacing, driven by meteorological input from a GCM, to conduct simulations with ^{210}Pb, a surrogate for aerosol. *Luecken et al.* [1991] used an Eulerian hemispheric model with 5° × 3° horizontal grid spacing, explicit descriptions of cloud and chemical processes, and driven by meteorological input from a GCM to simulate the transport of sulfur from North America and Europe across the North Atlantic Ocean during 30-day periods in January and July.

Results from the *Langner and Rodhe* [1991] model were compared with long-term point measurements, with ship and aircraft campaign measurements, and with optical depth measurements [*Langner et al.*, 1993]. Because the model uses monthly averaged meteorological data, it is unable to capture the temporal and spatial variability of the campaign measurements; even when compared to monthly averaged observations the model fails to correctly capture the seasonal variations exhibited by the observational data. *Galloway et al.* [1992] compared the January and July monthly averaged sulfur and nitrogen levels simulated by several of the above listed models at locations around the North Atlantic to monthly averaged observations at these locations. Although all models predicted similar sulfate concentration patterns over large geographic areas, results at the selected locations varied between models. Models using meteorological data generated by GCM's were able to capture the temporal variability of sulfate fields better than the models using averaged meteorological data, but both types were unable to accurately represent the variability of the observed data for specific years, and obviously cannot be compared to individual observations.

An alternative approach to these models that allows the simulation of the high variability of the sulfate fields is the use regional-scale models. A number of these regional-scale models are currently in use. The regional acid deposition model (RADM) [*Chang et al.*, 1987] is an Eulerian model with 80-km horizontal grid spacing and detailed sulfur and oxidant chemistry, driven by results from a mesoscale meteorological model. RADM has been adapted for use in Europe [*Hass et al.* 1991]. *Carmichael and Peters* [1984a, 1984b], developed an Eulerian model with 80-km horizontal grid spacing and detailed sulfur and oxidant chemistry, driven by meteorological fields derived from the 12-hour rawindsonde data provided by the National Weather Service. *Venkatram and Karamchandani* [1986] developed an Eulerian model with approximately 100-km horizontal grid spacing and detailed sulfur and oxidant chemistry, driven by output from a diagnostic module that combines information from the Canadian Meteorological Center large-scale numerical weather prediction model with information from a high-resolution boundary layer model. All these models have been reasonably successful in describing episodic sulfate loading and acid deposition at the regional scale and in capturing the short-term variability of these fields; however, subhemispheric- to global-scale simulations over extended periods are too computationally demanding.

Simulation and source attribution of sulfate concentrations and wet deposition at specific times and locations over the northern hemisphere have been addressed by *Tarrason and Iversen* [1992]. These investigators used a hemispheric Eulerian model with 10 vertical isentropic levels and a 300-km horizontal grid spacing to study the influence of anthropogenic SO_2 emissions from North America over western Europe. Meteorological data were taken from the 12-hour synoptic analyses of the U.S. National Meteorological Center (NMC); precipitation amounts were calculated by a diagnostic model using the NMC data. Dry

deposition velocities (0.8 cm s^{-1} for SO_2 and 0.1 cm s^{-1} for sulfate) at 1 m were modified via the use of an aerodynamic bulk diffusion coefficient and the surface wind speed to obtain values pertinent to the top of the surface layer. Wet deposition was calculated as the product of the precipitation rate, the pollutant concentration in air, and a scavenging efficiency, defined in terms of in-cloud and below-cloud scavenging ratios. A latitudinally and seasonally dependent linear oxidation rate was applied to the gas phase reaction of SO_2; aqueous phase chemistry was parameterized by increasing the scavenging ratio of particulate sulfate inside clouds. Monthly averaged model results are comparable to averages of measured sulfate surface concentrations at several stations along western land points of Europe, and to averaged results of observational campaigns measuring SO_2 and sulfate along the eastern coast of North America.

In this paper we describe a regional- to global-scale Eulerian transport and transformation model of sulfur emissions which was developed to bridge the gap between the hemispheric- to global-scale and the regional-scale models described above. The model uses fine horizontal grid spacing (1.125°) and temporal resolution (6 hours) to represent transport winds and precipitation and to resolve the temporal and spatial variability of the sulfate fields at scales much finer than previous global models. It is driven by meteorological data derived from observations, so that concentrations can be simulated at actual times and locations. We focus here on the North Atlantic and adjacent continental regions because the anthropogenic sulfate signal should be strong there, and should therefore be discernable in satellite measurements of clear-sky and cloud albedo. We report results of initial calculations for October and November of 1986 by presenting "snapshots" (results at specific times) and overall statistics on modeled sulfate concentrations and column burdens and on attribution of the burdens by source type (anthropogenic, biogenic), source region (North America, Europe) and oxidation pathway (primary, gas phase oxidation, aqueous phase oxidation). To assess the accuracy of model results, we compare results with measured surface concentrations. Finally, we characterize the time and space variability exhibited by the model results.

2. Description of the Model

The model employed in this study is based on the global chemistry model (GChM) [*Luecken et al.*, 1991]. The model solves material balances based on the continuity equations with the application of gradient-transport assumptions. To solve these equations, numerical approximations at any location (x, y, z) are considered mechanistically and dimensionally independent over short periods of time (time step is 1 hour) according to the operator splitting technique, also known as the "locally one dimensional" approximation [*Yanenko*, 1971]. Spatial integrals of the transport are approximated using the area-preserving flux form developed by Bott [*Bott*, 1989; *Easter*, 1993]. Dry deposition is represented as the lower boundary condition for the vertical transport. The integration procedure for each transformation term (gas and aqueous phase chemical conversions) treats loss terms as exponential decay terms [*Hesstvedt et al.*, 1978]. The local abundance of chemical species is represented as a mixing ratio to eliminate dependence on changes in pressure, and is expressed as parts per billion (ppb, equivalent to nmol per mole of air) for both gaseous and aerosol species. A schematic of the model components is presented in Figure 1; Table 1 summarizes the input data required by the model. In this section we describe the model, the new features implemented for this work, the data sources and the data processing required. Additional details on the development and implementation of the model are given by *Benkovitz* [1994].

2.1. Meteorological Data

Two existing archives of meteorological data sets were examined as candidates for use in this study: the U.S. National

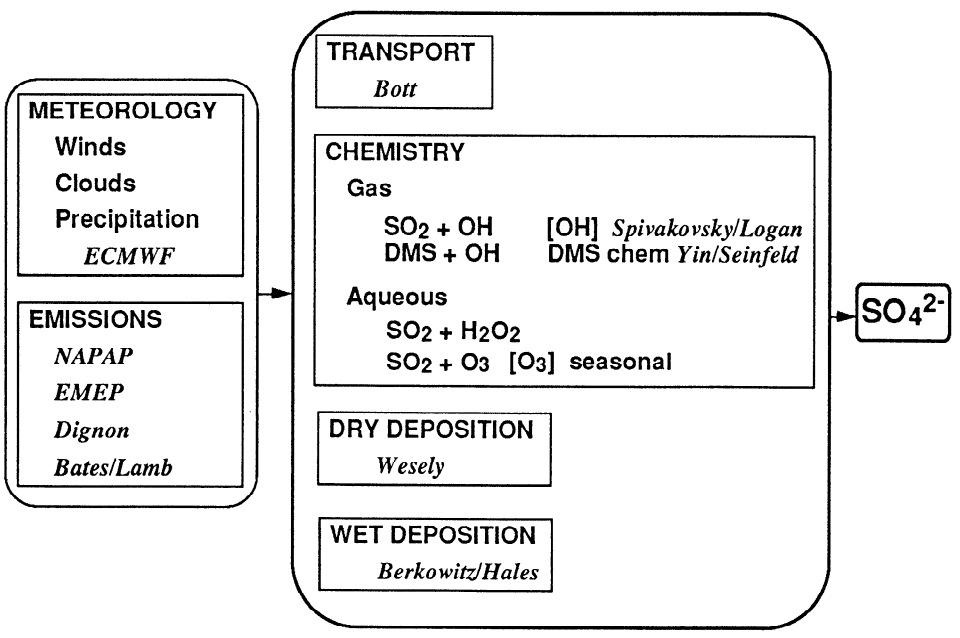

Figure 1. Schematic of the model components showing the different modules and summarizing the processes simulated in each one.

Table 1. Input Variables Required by the Transport and Transformation Model and by the Dry Deposition Velocity Calculations

Transport And Transformation Model	
2-D Fields (1.125° × 1.125°)	3-D Fields (15 Vertical Levels)
Meteorology	
Convective cloud cover	u component of wind
Convective precipitation	v component of wind
Stratiform cloud cover	w component of wind
Stratiform precipitation	Condensed moisture
Surface pressure	Temperature
Surface temperature	Specific humidity
Dry deposition velocity (SO_2, sulfate)	K_{zz}
Chemistry	
$[O_3]$ values	Rate constants
	[OH]
	$[H_2O_2]_{max}$ and production rate
Emissions	
DMS	SO_2, sulfate
Dry Deposition Velocity Calculations	
Land use	
Precipitation	
Seasonal albedo	
Seasonal categories	
Snow cover	
Surface latent heat flux	
Surface pressure	
Surface relative humidity	
Surface sensible heat flux	
Surface total shortwave radiation	
Surface temperature	
Surface wind speed	

Weather Service (NWS) archive [*Trenberth and Olson*, 1988] and the European Centre for Medium-Range Weather Forecasts (ECMWF) archive [*ECMWF*, 1988]. Both institutions continuously run state-of-the-art weather forecasting models, and model results as well as analyzed data sets are archived. Although neither archive includes all the variables that are needed as input by the present model, the ECMWF archives include sufficient variables to permit the model inputs, as specified in Table 1, to be derived.

The ECMWF "first guess" data set consists of results from the forecast model, before assimilation of observational data; the assimilation process does not retain the cloudiness and precipitation data needed for running the present model. Data sets consist of two-dimensional fields, available in Gaussian grid or latitude/longitude coordinates (1.125° × 1.125° grid), and three-dimensional fields, available in spherical harmonics or latitude/longitude coordinates, with model η coordinates or pressure surfaces as the vertical coordinate.

Conversion of ECMWF analyses from the model coordinate system to pressure levels introduces errors in mass conservation which result in serious imbalances in the budgets of moisture, pollutants or other atmospheric tracers if the three-dimensional velocity fields from the pressure level data are used to transport these tracers [*Trenberth*, 1991]. Therefore, we use the ECMWF data in the original coordinate system, defined by [*Simmons and Struffing*, 1981; *ECMWF*, 1988]

$$p_{k+1/2} = A_{k+1/2} + B_{k+1/2} p_s$$

$$\eta_{k+1/2} = A_{k+1/2}/p_0 + B_{k+1/2}$$

where k is the ECMWF level number (0, 1, ... , n), $p_{k+1/2}$ is the pressure at the interface between levels k and k+1, $A_{k+1/2}$ and $B_{k+1/2}$ are constants, p_0 is a reference sea-level pressure, and p_s is the surface pressure. Necessary values of the constants are $A_{1/2} = B_{1/2} = A_{n+1/2} = 0$ (therefore, $p_{1/2} = 0$), and $B_{n+1/2} = 1$ (therefore, $p_{n+1/2} = p_s$). Other values were determined by fitting polynomials to functions of k/n with $p_0 = 1013.25$ hPa and a top level pressure of zero, and

$$\int_0^1 d\eta = 1$$

ECMWF levels are numbered 0 ($p_{1/2} = 0$) to 19 ($p_{19+1/2} = p_s$) [*ECMWF*, 1988]; here, levels are numbered in reverse order, corresponding to 1 for the first level above the surface, and the highest level, 15, corresponding to ECMWF level 5 (approximately 100 hPa). Pressures for the ECMWF half-levels and corresponding nomenclature for vertical levels in the present model are displayed in Figure 2.

The optimum time period satisfying constraints of availability of required meteorological data and of satellite observations to be used in subsequent comparisons was June 1985 to June 1987 inclusive; this study presents results for the months of October and November 1986. Appendix A describes analyses undertaken to compare meteorological data used in the simulations with the weather reports covering the modeled time period.

The vertical velocity ($\dot{\eta} = d\eta/dt$) and vertical profiles of cloud water are not explicitly provided by the ECMWF data set and therefore must be calculated for input to the model. Vertical velocities are calculated from the u and v components of the wind and the divergence at each vertical level [*ECMWF*, 1988].

To derive vertical profiles of cloud water for precipitating clouds, two models are applied using the available meteorological data, one for stratiform clouds and one for convective clouds. To estimate stratiform cloud water, a quasi-steady state precipitation-scavenging model [*Berkowitz et al.*, 1989] was applied. This model simulates horizontally uniform precipitation growing in a weak updraft. A uniform precipitation rate was applied to the stratiform precipitation data over the 6-hour ECMWF meteorological time interval; the model uses the ECMWF temperature and moisture profiles to define a cloud top, and adjusts a parabolic updraft profile until the resulting precipitation amount agrees with the ECMWF-derived data. Convective cloud water was calculated by applying the model of *Walcek and Taylor* [1986], using the convective precipitation amount provided in the ECMWF data set. The convective cloud is assumed to be composed of a mixture of air from below cloud base and above cloud top. Cloud base is defined as the lifting condensation level of the layer of air having the highest equivalent potential temperature. Cloud top is defined as the

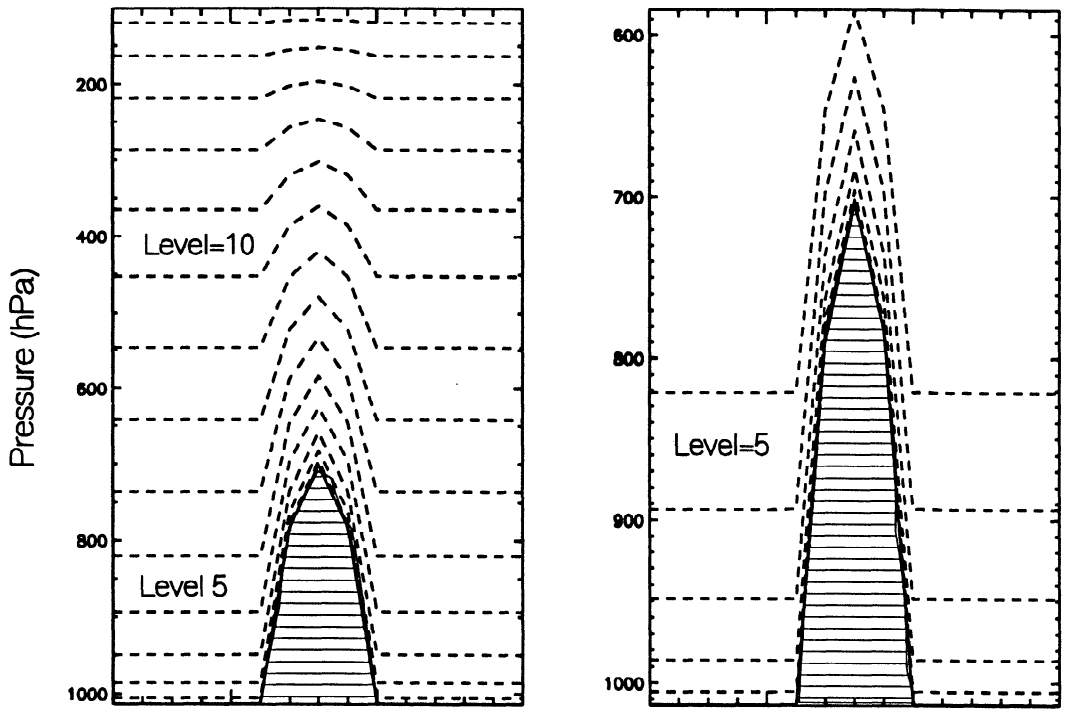

Figure 2. Distribution of half-level pressures for a sea level pressure of 1013.25 hPa, and corresponding nomenclature for the vertical levels in the transport and transformation model. Note response of levels to terrain features denoted by hashed areas. Left panel shows all 15 model levels; right panel shows detail of the terrain influence on the lower levels of the model.

level at which cloud base air, when lifted adiabatically, becomes 5°C cooler than the environment. At each level, the relative amounts of cloud-base and cloud-top air are selected so that the ratio of the cloud water concentration to its adiabatic value agrees with observations by *Warner* [1970]. Calculated values for vertical velocity and cloud water vertical profiles were incorporated into the meteorological data set and used as input to the model.

Values for the vertical eddy diffusivity, K_{zz}, are needed for the planetary boundary layer (PBL). Lacking a detailed PBL parameterization, the PBL was assumed to include layers 1 through 4, since the representative height of the interface between levels 4 and 5 is 1.7 km. A value of 1×10^5 cm^2 s^{-1} was chosen for K_{zz} in the PBL [*Pasquill*, 1976]. Because of the small thickness of model layer 1 (roughly 65 m), this value of K_{zz} and a 1-hour time step result in oscillatory behavior in the finite difference approximation to the diffusive transport equation. Since K_{zz} varies linearly with height near the surface [*Louis*, 1979], a smaller K_{zz} value of 0.25×10^5 cm^2 s^{-1} was used for level 1. Above the PBL, vertical turbulent transport was assumed negligible compared to other transport processes, and K_{zz} was set to zero.

2.2. Dry Deposition

Time- and location-dependent dry deposition velocities of SO_2 and accumulation-mode particulate sulfate were calculated as described by *Wesely* [1989]. A series resistance model approach is used, with deposition velocity being inversely proportional to the sum of three resistance terms: aerodynamic resistance, resistance to transport across the atmospheric sublayer in contact with surface elements, and a surface (or canopy) resistance. Aerodynamic and sublayer resistances are calculated based on micrometeorological parameters [*Sheih et al.*, 1986], surface resistances are estimated on the basis of studies summarized by *Wesely* [1989]. Data needed for these calculations, listed in Table 1, include meteorological data from ECMWF, the seasonal 1° × 1° global albedo files of *Matthews* [1985], land use classifications derived from *Wilson and Henderson-Sellers* [1985], and seasonal categories developed by *Wesely* [1989]. Details of the implementation and results are given by C. M. Benkovitz and M. Wesely (manuscript in preparation, 1994). Histograms of dry deposition velocities over land and ocean areas for the domain and period modeled are presented in Figure 3. Dry deposition velocities for SO_2 over ocean areas of the model domain had a 90th percentile value of 1.47 cm s^{-1}, with an area-weighted average value of 0.77 cm s^{-1}; over land areas, deposition velocities had a 90th percentile value of 0.39 cm s^{-1}, with an area-weighted average value of 0.17 cm s^{-1}. Dry deposition velocities for sulfate over ocean areas had a 90th percentile value of 0.093 cm s^{-1}, with an area-weighted average value of 0.09 cm s^{-1}; over land areas deposition velocities had a 90th percentile value of 0.24 cm s^{-1}, with an area-weighted average value of 0.11 cm s^{-1}. The sulfate deposition velocities are valid for particles roughly 0.1 to 3 μm in diameter [*Wesely*, 1989].

These results can be compared with those obtained by *Voldner et al.* [1986], who conducted a literature survey of dry deposition observations and corresponding estimates of deposition velocity; results represent the meteorological conditions and surfaces sampled and can be summarized as follows. For SO_2, deposition velocities ranged between 0.16 and 4 cm s^{-1} over water, and between 0.1 and 2.5 cm s^{-1} over land. For sulfate, deposition velocities ranged between 0.13 and 0.65 cm s^{-1} over water, and between 0.03 and 1.45 cm s^{-1} over land. *Sirois and Barrie* [1988]

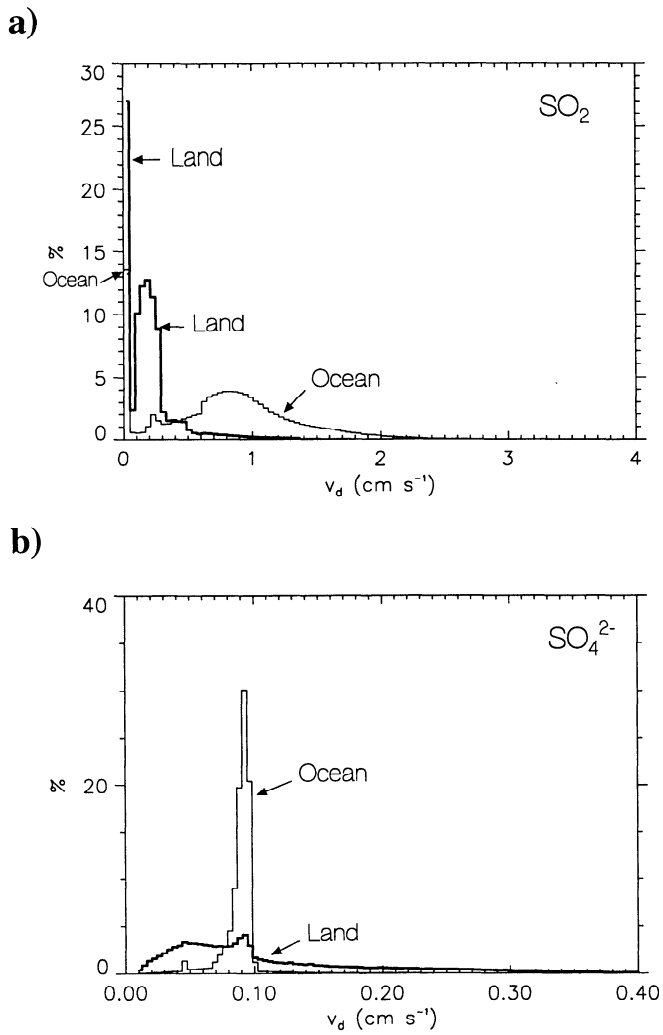

Figure 3. Histogram of deposition velocities for October 1 to November 15, 1986, for the model domain. (a) SO_2. The high peaks at the low end of the distributions (14% for ocean; 27% for land) reflect the low deposition velocities over ice/snow and the imposition of a minimum deposition velocity value for stable conditions, both situations prevalent over the northern areas of the modeling domain. (b) Sulfate.

estimated monthly area average dry deposition velocities of SO_2 and sulfate for six sites of the Canadian monitoring network; for the month of October, their estimates ranged between 0.20 and 0.35 cm s^{-1} for SO_2, and between 0.33 and 0.42 cm s^{-1} for sulfate. Results are within the ranges of these estimates, except for the Sirois and Barrie sulfate deposition velocities, which are at the extreme high end of our distribution. Results for sulfate can also be compared to those obtained with a model to predict dry deposition velocities of particles over water [*Williams*, 1982; *Slinn*, 1983]. The model includes a postulated, theoretical effect of the broken surface of water associated with breaking waves under high wind speeds to show that the deposition velocity of particles ranging in size from 0.1 to 1.0 μm in diameter could increase from values near 0.02 cm s^{-1} for low wind speeds to near 1 cm s^{-1} at wind speeds of 20 m s^{-1}. These types of predictions, however, do not seem to have been tested yet by field experiments.

2.3. Cloud Processes

Clouds in the model provide an environment for aqueous chemical reactions, provide wet removal, and in the case of convective clouds, supply mixing and subgrid-scale vertical motions. The ECMWF meteorological fields specify convective cloud cover; low, medium, and high stratiform cloud cover; convective precipitation rate; and stratiform precipitation rate. The stratiform cloud module is activated when the stratiform cloud cover (defined as the maximum of the low, medium, and high cloud covers) exceeds the convective cloud cover in a grid cell, and the stratiform precipitation rate exceeds 0.1 mm h^{-1}. If these conditions are not met, and the convective precipitation rate exceeds 0.1 mm h^{-1}, the convective cloud module is activated. These modules are based on the cloud models used to calculate the vertical profiles of cloud water, described in section 2.1. Otherwise clouds are absent; reactions in nonprecipitating clouds are not included in this treatment because vertical profiles of cloud water for these conditions cannot be accurately estimated with the cloud models used.

2.4. Wet Removal

Wet removal of a soluble species is evaluated using a removal of cloud water from a vertical column in time step Δt, determined by the precipitation amount and column integral of cloud water. The column integral of cloud water, L, (mol m^{-2}) is

$$L = \frac{p_s}{gM_a} \int_{h_1}^{h_2} r_{cw} d\eta$$

where r_{cw} is the cloud water mixing ratio (moles H_2O per mol air), g is the acceleration of gravity, M_a is the molecular weight of air, p_s is the surface pressure, h_1 is the cloud base height and h_2 is the cloud top height. Fractional cloud water removal in a model time step Δt, e_{wet}, is

$$e_{wet} = \frac{P\Delta t}{L}$$

where P is the surface precipitation rate over the cloudy fraction of the grid column. The change in the mixing ratio of species m in time step Δt, due to wet removal is given by

$$\Delta r_{m,cw} = -e_{wet} r_{m,cw}$$

where $r_{m,cw}$ is the mixing ratio for the portion of species m dissolved in cloud water. The column integral of dissolved material is

$$B_{m,cw} = \frac{p_s}{gM_a} \int_{h_1}^{h_2} r_{m,cw} d\eta$$

and the wet deposition amount of species m for the grid column is thus given by

$$D_{m,wet} = e_{wet} B_{m,cw}$$

2.5. Species and Reactions Represented in the Model

Sulfur species whose concentrations are computed by the model are listed in Table 2. In order to distinguish the contribution from different source regions to the resulting sulfate fields, emissions from three different regions, west of 30°W

Table 2. Sulfur Species Represented by the Model

Source	SO_2		Sulfate			DMS	MSA
	Primary	Gas Phase Oxidation	Primary	Gas Phase Oxidation	Aqueous Phase Oxidation	Primary	Gas Phase Oxidation
West of 30°W Anthropogenic	${}_{NA}^{p}SO_2$		${}_{NA}^{p}SO_4^{2-}$	${}_{NA}^{g}SO_4^{2-}$	${}_{NA}^{a}SO_4^{2-}$		
East of 30°W Anthropogenic	${}_{Eu}^{p}SO_2$		${}_{Eu}^{p}SO_4^{2-}$	${}_{Eu}^{g}SO_4^{2-}$	${}_{Eu}^{a}SO_4^{2-}$		
Biogenic		${}_{Bio}^{g}SO_2$		${}_{Bio}^{g}SO_4^{2-}$	${}_{Bio}^{a}SO_4^{2-}$	DMS	MSA
External	${}_{Ext}SO_2$		${}_{Ext}^{p}SO_4^{2-}$	${}_{Ext}^{g}SO_4^{2-}$	${}_{Ext}^{a}SO_4^{2-}$		

anthropogenic (designated North American, subscript NA), east of 30°W anthropogenic (designated European, subscript Eu), and biogenic sources (subscript Bio), plus material transported from outside the model domain (designated external, subscript Ext), and their products, are computed as individual species. In addition, we distinguish the sulfate resulting from gas phase oxidation of SO_2 by OH from that resulting from aqueous phase oxidation, since sulfate generated by OH oxidation may form new particles via homogeneous nucleation, whereas aqueous phase oxidation does not generate new particles, but rather adds mass to particles which generated the cloud droplets.

2.6. Chemical Reactions

The chemical reactions represented in the model are gas phase oxidation of SO_2 and dimethyl sulfide (DMS) initiated by OH, and aqueous phase oxidation of SO_2 by H_2O_2 and O_3. The chemical reactions in the generation of H_2O_2 and the concentrations of OH and O_3 needed for the chemical reactions included in the model are parameterized as described in the following sections.

2.6.1. Gas Phase Reactions. Oxidation of SO_2 by OH is represented as a pseudo-first-order reaction,

$$SO_2 + OH \rightarrow SO_4^{2-}$$

Rate constants as a function of temperature and pressure are taken from *NASA* [1991]. Concentrations of OH were obtained from the photochemical model calculations of *Spivakovsky et al.* [1990], who computed three-dimensional 24-hour average OH concentrations every 5 days for 1 year, on a 10° by 8° grid at nine pressure levels. This model used meteorological conditions derived from a GCM, and climatologies for CO, nitrogen oxides, O_3 and CH_4 derived from observations. Using these OH concentrations allows inclusion of the influence of such variables as the length of daylight and solar zenith angle on oxidant concentrations, and representative concentrations of OH-influencing chemicals, albeit for a climatological October, rather than for conditions specific to October and November of 1986. These parameters represent the most important source of systematic variability in oxidant concentrations.

Oxidation of DMS by OH is also represented as a pseudo-first-order reaction,

$$DMS + OH \rightarrow \alpha SO_2 + (1-\alpha)\,MSA$$

where MSA (for methanesulfonic acid) designates a nonsulfate aerosol product having removal processes identical to those for sulfate; $(1-\alpha)$ ranges from 0.07 to 0.20, increasing with decreasing temperature over the range 315°K to 240°K. The mechanism for this simplified DMS chemistry, derived mainly from the work of *Yin et al.* [1990a, 1990b], is summarized in Appendix B.

H_2O_2 is generated in the gas phase at a fixed rate until a maximum concentration, $[H_2O_2]_{max}$ is reached; vertical profiles for $[H_2O_2]_{max}$ and the H_2O_2 generation rate were adapted from *Logan et al.* [1981]. At the surface, $[H_2O_2]_{max}$ is set to 1.4 ppb, and the generation rate is set to 0.021 ppb h^{-1}; these values are maintained for the lowest 1 km of the atmosphere and are then decreased by a factor of 2 every 3 km in height.

2.6.2. Aqueous-Phase Reactions. At the beginning of each time step, gases and aerosols from the cloud-base and cloud-top source regions are mixed into each layer in the cloudy fraction of the grid, in relative amounts determined by the mixing used to define the cloudwater concentrations, as described in section 2.3. Soluble aerosols (sulfate, MSA) are assumed to be taken up immediately and completely into cloud water [*ten Brink et al.*, 1987]. Soluble gases (SO_2, O_3, H_2O_2) dissolve in cloud water based on their solubilities and undergo aqueous chemical reactions over the cloud lifetime. At the end of the time step, a fraction of the cloud water and the dissolved chemical species within it are removed as precipitation, as described in section 2.4.

Reactions represented in the aqueous-phase chemistry mechanism are oxidation of SO_2 by H_2O_2 and O_3. Oxidation of SO_2 by H_2O_2 is treated as going immediately to completion, limited by the lesser of either the SO_2 or the H_2O_2 concentrations [*Daum*, 1988]. When the reaction is H_2O_2 limited, SO_2 from each source type is oxidized relative to its fraction of the total. Oxidation of SO_2 by O_3 proceeds only if there is any residual SO_2 after reaction with H_2O_2. The effective Henry's law coefficient for the equilibrium partitioning of SO_2 into cloud water is calculated assuming a fixed pH for cloud water of 4.5, and the SO_2 oxidation is calculated as a pseudo-first-order reaction of the gaseous SO_2. An aqueous phase rate constant of 1.68×10^{-3} s^{-1} was derived from *Erickson et al.* [1977] and *Easter and Luecken* [1988], assuming $[O_3] = 37$ ppb; see also *Schwartz* [1988b].

2.7. Initial Conditions and Boundary Fluxes

The model domain chosen covers the region 140.6°W to 61.9°E and 12.4°N to 81.0°N, and includes North America, the North Atlantic Ocean, Europe, the Middle East and the northern part of Africa. Because this domain is not global, it is necessary to assume external concentrations in order to calculate fluxes into the domain. The following concentrations were selected for use in evaluating boundary fluxes. SO_2 concentrations, presented in Figure 4a, were adapted from *Bandy et al.* [1992], *Ferek et al.* [1991] and *Berresheim et al.* [1990]. Concentrations of 40 ppt (pmol/mole air) were used from the surface to 5 km, decreasing to 15 ppt at 15 km, and decreasing to 10 ppt at 30 km. Sulfate concentrations, also presented in Figure 4a, were adapted from *Hofmann* [1990] and *Sedlacek et al.* [1983]. Concentrations are at 120 ppt at the surface, decreasing to 64 ppt at 8 km, constant to 15 km, increasing to 210 ppt at 20 km. The column burden for this sulfate concentration profile is 26 μmol m^{-2}; the corresponding aerosol optical depth, estimated using an empirical value for the extinction coefficient of moist sulfate aerosol of 8.5 $m^2 g^{-1} (SO_4^{2-})$, (816 $m^2 mol^{-1}$) [*Charlson et al.*, 1991], is 0.024. This optical depth is comparable to aerosol optical depth reported for baseline conditions at Cape Grim, Tasmania, by *Forgan* [1987]; averages for May 1985 (austral fall) varied from 0.029 at 368 nm to 0.032 at 675 nm. H_2O_2 concentrations, presented in Figure 4b, are 75% of the maximum concentrations described in section 2.6. DMS concentrations, also presented in Figure 4b, were adapted from *Berresheim et al.* [1990]; concentrations are 30 ppt at the surface, decreasing to zero at 3 km.

A related issue is determination of the time required for memory of initial conditions to vanish (startup time). In order to determine the startup time, two test runs were conducted; one with initial concentrations in the domain set to zero and another with initial concentrations set to the background values described above. After 282 simulation hours (approximately 12 days), the difference in the total mass in the domain when using the two sets of initial concentrations was less than 0.1% for SO_2 and less than 5% for sulfate. For this reason, we report results starting on October 13 for model runs initiated on October 1 with initial concentrations of zero for all species.

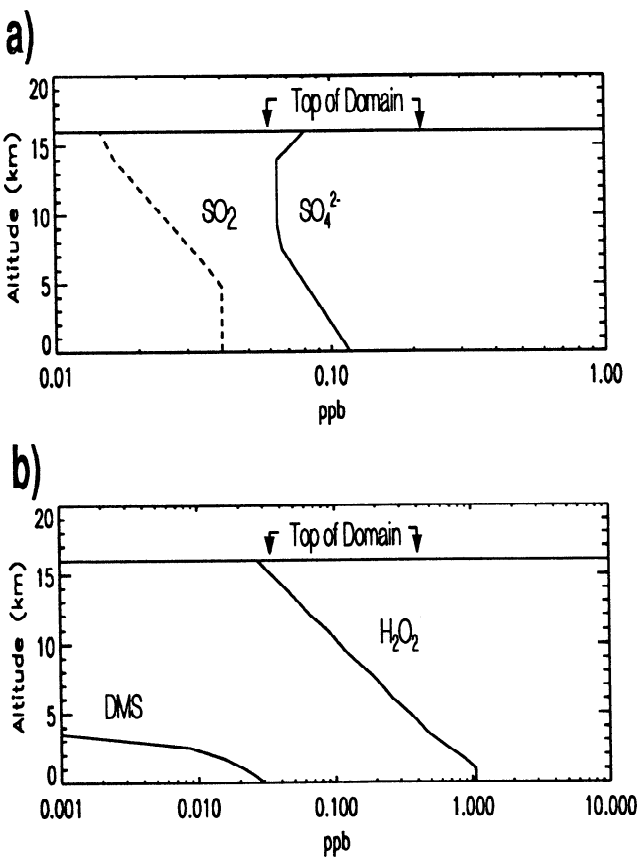

Figure 4. Concentrations used to evaluate fluxes into the model domain. (a) SO_2 and sulfate. (b) H_2O_2 and DMS.

2.8. Emissions

2.8.1. Anthropogenic Emissions. Anthropogenic emissions were derived whenever possible from detailed regional inventories compiled for the National Acid Precipitation Assessment Program (NAPAP), for emissions from the U.S. and Canadian sources, and for the European Monitoring and Evaluation Program (EMEP), for emissions from Europe.

The NAPAP 1985 version 2 inventory [*Saeger et al.*, 1989] consists of annual emissions of SO_2 and primary sulfate, with temporal factors available to estimate seasonal allocations. The data are available as individual points for large stationary sources, and on a county basis for smaller stationary sources and mobile sources. Emissions from this inventory were distributed to the ECMWF-specified grid as follows. Based on the representative heights for the first three levels above ground in the model (65 m, 228 m and 540 m), 60 and 220 m were selected as the dividing points for the vertical distribution of emissions. Emissions from large stationary sources were assigned according to their latitude/longitude and distributed to the three vertical levels based on stack height information. Emissions from smaller stationary and mobile sources were apportioned to the 20 × 20 km grid used for RADM based on gridded population [*Modica and Dulleba*, 1990]; this grid was then aggregated to the ECMWF-specified grid, with all emissions assigned to the lowest vertical level. Total emissions from this inventory are 387 Gmol yr^{-1} for SO_2 and 5.6 Gmol yr^{-1} for primary sulfate (1.4% of the total sulfur emissions).

The EMEP inventory [*Iversen et al.*, 1990] consists of annual data for 1980; these data were updated to 1985 (D. Simpson, Norwegian Meteorological Institute, Oslo, personal communication, 1992). The 1985 inventory provides sulfur emissions on the EMEP 150 × 150 km polar stereographic hemispheric grid with two vertical levels, defined at below and above 100 m. European modeling groups assume that 5% of these emissions are primary sulfate [*Eliassen*, 1978; *Eliassen and Saltbones*, 1983]; we have used this value to apportion emissions between the two species for this inventory. However, in view of measurements on the relative magnitude of SO_2 and primary sulfate emissions [*Dietz and Wieser*, 1983] indicating that primary sulfate emissions rarely exceed 2.5% of the sulfur emissions, the 5% allocation probably overestimates the primary sulfate contribution in this inventory. Emissions were converted to the ECMWF meteorological grid by reapportioning each EMEP grid cell to the corresponding ECMWF grid cells, with vertical distribution within the first two model levels. Total emissions from this inventory are 680 Gmol yr^{-1} for SO_2 and 35.7 Gmol yr^{-1} for primary sulfate.

Emissions for areas not covered by the regional inventories were taken from the global inventory of SO_2 emissions from fuel combustion developed by Dignon [*Dignon and Hameed*, 1985; *Dignon*, 1992], allocated to a 1° × 1° latitude/longitude grid based on population. All sulfur computed by this inventory is assumed to be emitted as SO_2; that is, there are no primary

sulfate emissions. The 1° gridded emissions were converted to the ECMWF meteorological grid by dividing the 1° cells into 0.125° cells and reaggregating these to the 1.125° grid. In the model domain, emissions from this inventory totaled 94 Gmol yr^{-1} for areas west of 30°W and 251 Gmol yr^{-1} for areas east of 30°W.

Emissions in the NAPAP inventory show very little seasonal variability [*Saeger et al.*, 1989]. For the EMEP inventories, European modeling groups assume average monthly emissions modified by a sinusodial distribution over the seasons, with maximum in January and minimum in July [*Berge*, 1990]. No information on seasonality was available in the Dignon inventory. For the October-November simulations, we have assumed that daily emissions in the domain are 1/365 of the yearly emissions.

The geographic distribution of anthropogenic emissions in the model domain is presented in Plate 1a. The distribution is highly nonuniform; note the use of a logarithmic scale, which covers over 3 orders of magnitude. The highest emissions are over the industrialized areas of North America and Europe; emissions in other areas generally follow population patterns.

2.8.2. Biogenic Emissions. The principal biogenic emissions of reduced sulfur compounds are oceanic DMS emissions, with lesser terrestrial emissions of DMS, dimethyl disulfide (DMDS), H_2S, carbonyl sulfide (OCS) and CS_2 [*Bates et al.*, 1992]. Oceanic DMS emissions for winter and summer were presented as totals in several latitude bands for each of three ocean basins: Atlantic, Pacific and Indian; emissions for the Mediterranean Sea were neglected (T. Bates, Pacific Marine Environmental Laboratory, Seattle, Washington, personal communication, 1992). For October-November, emissions were taken as halfway between the winter and summer values. To distribute these emissions within the latitude bands, 1° x 1° gridded pigment concentrations from the CZCS (Z. Kolber, Brookhaven National Laboratory, Upton, New York, personal communication, 1992) were used. A composite global map of the pigment concentrations for the month of October was obtained from all available CZCS data; concentrations for areas with no data were estimated based on the average of the four closest neighbors. The DMS emissions in each oceanic latitude band were then distributed to the 1° × 1° grid proportional to the pigment concentration, while preserving the total emissions values of Bates et al. Emissions for the Mediterranean Sea on this 1° × 1° grid were estimated using an average of the summer and winter flux for the Atlantic Ocean. The 1° × 1° gridded emissions were then converted to the ECMWF grid as described above.

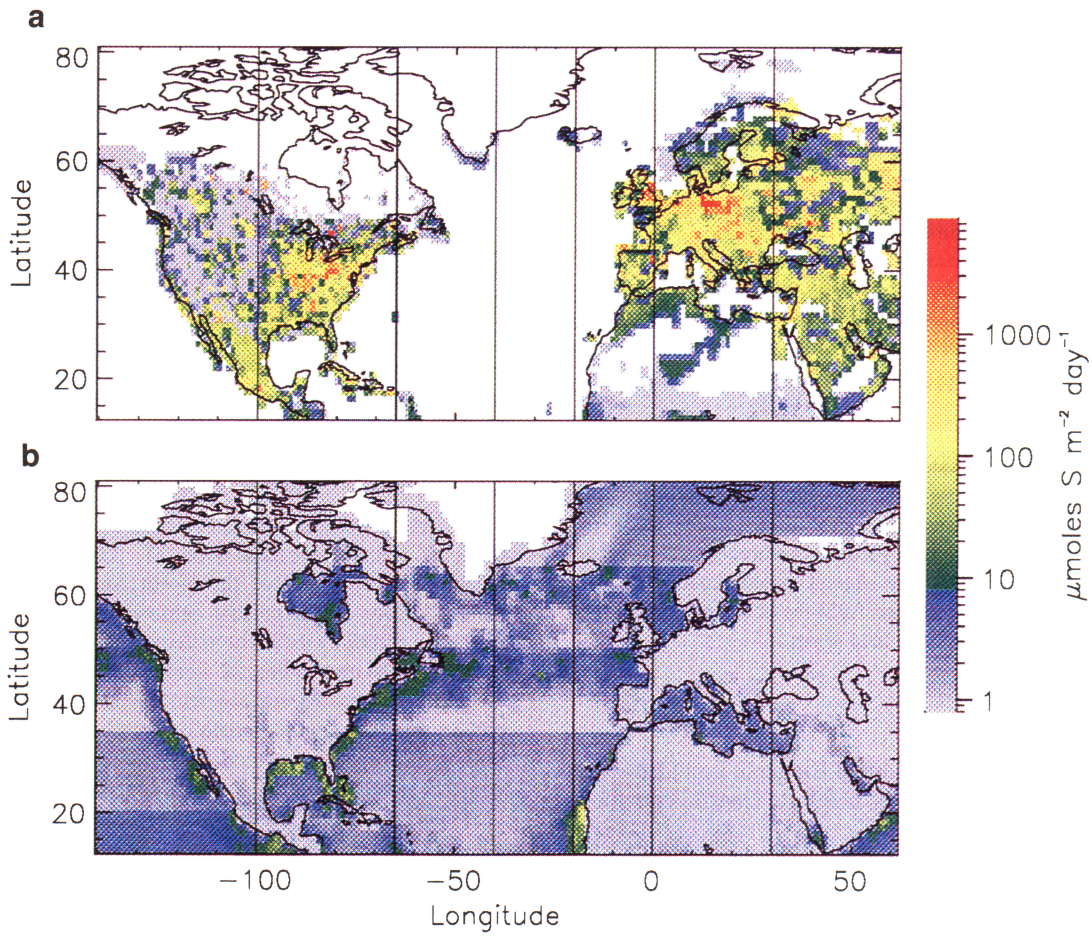

Plate 1. Emissions fluxes within the model domain. White denotes areas with zero emissions. (a) Fluxes from anthropogenic sources. (b) Fluxes from biogenic sources. The latitude band structure of the oceanic DMS emissions given by Bates et al. is still apparent after distribution proportional to CZCS data and reallocation to the model grid, introducing discontinuities in these emissions. Longitudinal bands used in source attribution are indicated: 100°W to 65°W, 65°W to 40°W, 40°W to 20°W, 20°W to 0°, and 0° to 30°E. Note the logarithmic scale used.

Biogenic emissions of sulfur compounds from land sources on a 1° by 1° grid by season were calculated using the methodology of Lamb [*Bates et al.*, 1992]. Emissions are estimated based on land use [*Wilson and Henderson-Sellers*, 1985], average seasonal temperature [*Shea*, 1986] and biomass conversion factors [*Zimmerman*, 1979] using the Michaelis flux rate algorithm. Table 3 presents global emissions of sulfur compounds from biogenic land sources.

Because of the low emissions, DMDS and CS_2 are not included in the model calculations. The main oxidation path for OCS, DMS and H_2S is initiated by the gas phase reaction with the OH radical. Rate constants for these reactions are presented in Table 3. OCS reactions were not included in the model calculations because its reaction rate with OH is slow. Since the reaction rate constant of H_2S with OH is similar to that of DMS, emissions of H_2S were combined with those of DMS and treated as DMS. Although this introduces a small error in the distribution of oxidation products between sulfate and MSA, since oxidation of H_2S obviously produces no MSA, the total aerosol burden is not greatly affected; approximately 5% excess MSA is estimated to result in the model domain.

The geographic distribution of biogenic emissions in the model domain is presented in Plate 1b. These emissions are much more uniformly distributed than anthropogenic emissions, with the highest emissions located in high productivity coastal areas. The latitude band structure of the oceanic DMS emissions presented by Bates et al. is still apparent, introducing discontinuities in these emissions.

2.8.3. Volcanic Emissions. In order to obtain an estimate of the possible magnitude of sulfur emissions from volcanoes, volcanic emissions in the model domain for 1980 were extracted from *Spiro et al.* [1992]. Because 1986 was a quiescent year for large volcanic eruptions [*Hofmann*, 1990], we examined emissions from degassing volcanoes only. For the period October 1 to November 15, 1980, emissions from degassing volcanoes represent approximately 11% of the biogenic and 0.6% of anthropogenic sulfur emissions in the model domain; consequently, volcanic emissions were omitted from the inventory.

2.8.4. Emissions Summary. Emissions in the model domain are summarized in Table 4. The total anthropogenic emissions are almost 18 times the total biogenic emissions and exhibit a much more localized geographic distribution, as seen by comparing the two panels of Plate 1. Anthropogenic emissions in the area east of 30°W are almost twice those west of this longitude. Biogenic emissions from the ocean are almost 6 times the biogenic emissions from land areas.

Table 3. Estimates of Global Biogenic Land Emissions of Reduced Sulfur Species and Rate Coefficients for Reaction with OH at 298°K

Compound	Emissions		$k_{[OH]}$
	Gg S yr^{-1}	Gmol S yr^{-1}	$cm^{-3}\,s^{-1}$
OCS	272.0	8.5	1.90×10^{-15}
CS_2	23.1	0.8	1.20×10^{-12}
DMDS	5.7	0.2	
DMS	213.2	6.7	5.89×10^{-12}
H_2S	920.2	28.9	4.70×10^{-12}
Total	1434.2	45.1	

Table 4. Emissions in Modeling Domain

	SO_2	SO_4^{2-}	DMS	H_2S	Total
Anthropogenic					
West of 30°W	481	6			487
East of 30°W	932	36			968
Biogenic					
Ocean			71		71
Land			2	10	12
Total	1413	42	73	10	1538

Biogenic emissions of DMS and H_2S were combined and follow the DMS chemistry. Units are Gmol S yr^{-1}.

2.9 Computer Use

Debugging and trial runs for the model computer codes were carried out on SUN SPARC and IBM RS/6000 platforms. Production runs were carried out on a CRAY C90 at the National Energy Research Supercomputer Center (NERSC), Lawrence Livermore National Laboratory, and require approximately 0.9 min of CPU time for each simulation hour. Computer codes have not been optimized for any particular platform.

3. Results

A model simulation was carried out for October 1 to November 15, 1986; concentrations of all species listed in Table 2 were captured every 6 hours as functions of location (longitude, latitude, and vertical level). Sulfate column burdens (vertical column integral of concentration) were calculated; for the biogenic emissions, both sulfate and MSA were considered. Various statistics were generated for the last 34 simulation days (October 13 to November 15), after start-up transients had become minimal. In this section we present examples of geographic distributions of sulfate concentrations and column burdens on specific dates, vertical meridional sections of concentrations at specific longitudes and times, and time series of burdens at specific locations.

3.1. Analysis of Results at Specific Times

We first present results at two specific times: October 15 at 0600 UT and October 22 at 0600 UT. These times were chosen because the influence of the North American and European source regions on the column burdens over the North Atlantic displayed distinctly different patterns. We interpret these results in terms of the meteorological conditions driving the model.

Figure 5 presents surface winds and the synoptic weather pattern over the model domain on October 15 at 0000 UT. To outline the geostrophic wind flow, we display in Figure 5a the constant height contour for 5500 gpm (geopotential meters, a characteristic height for the 500-hPa surface). High-pressure systems are located over the western United States and Greenland, and low-pressure systems are located at 34°W, 44°N, over northern Quebec and off the eastern coast of Greenland. A cold front is situated off the eastern coast of North America, a smaller cold front is situated over eastern Quebec, and cold and warm fronts are associated with the low pressure systems in the Atlantic. The 500-hPa flow leaving North America is zonal across the Atlantic, turning into a ridge system over Scandinavia. Precipitation (Figure 5b) is associated with the cold fronts over eastern North America, and with the fronts over the North

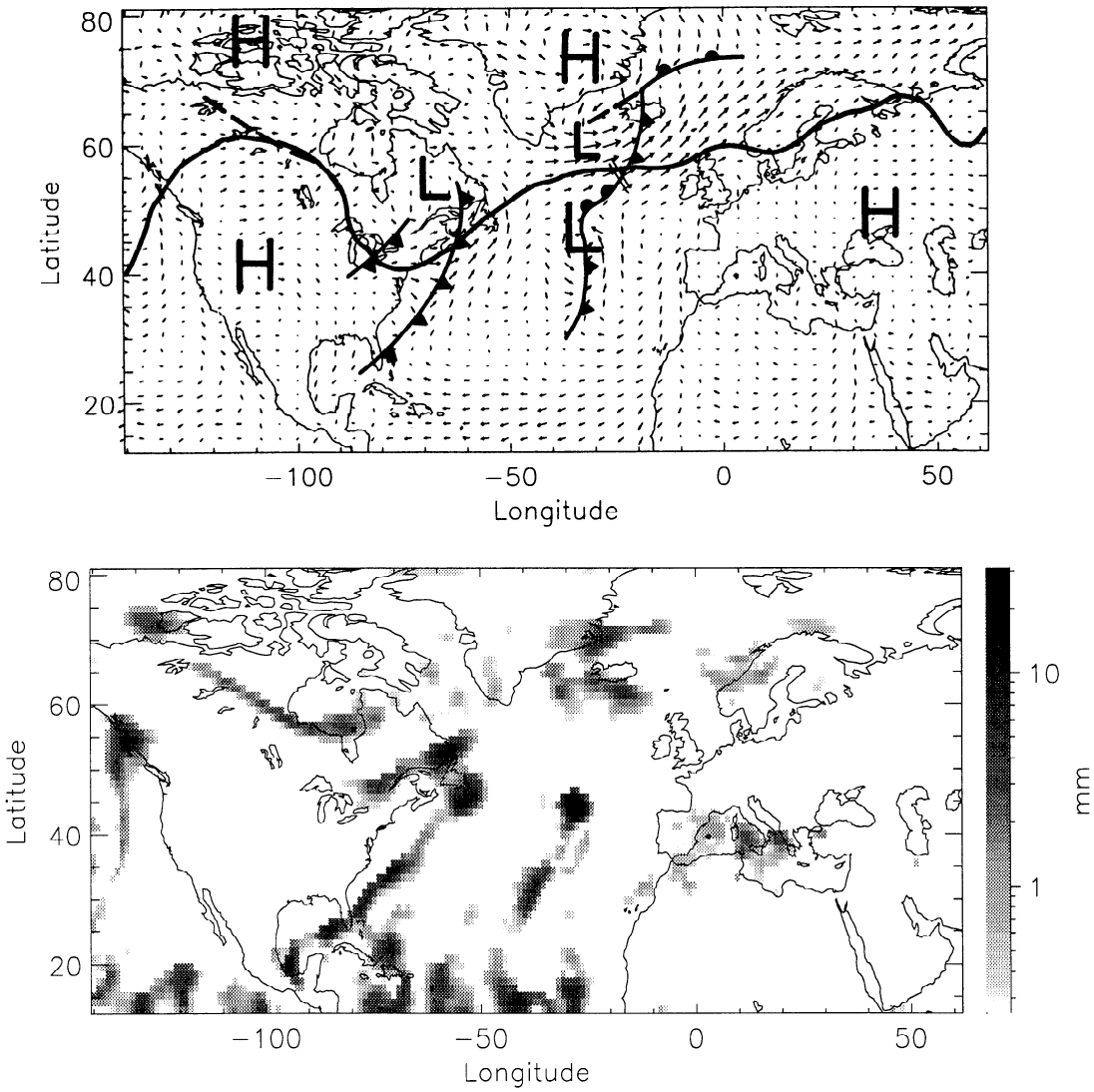

Figure 5. Weather maps for October 15, 1986, 0000 UT. (a) Surface wind vectors and synoptic weather. Solid lines are constant height lines for the surface at 5500 geopotential meters (gpm, a characteristic height for the 500-hPa surface). (b) Precipitation amounts in previous 6 hours.

Atlantic. Most of Europe is precipitation free, except for scattered areas over the Mediterranean Sea and over Scandinavia. There are scattered areas of precipitation in the subtropical regions west of 20°W.

The surface winds and synoptic pattern on October 22 at 0000 UT (Figure 6) are more complex. There are several high- and low-pressure centers and associated fronts; the major features are a low-pressure system in the mid North Atlantic at approximately 50°W, 40°N, a high-pressure system off the western coast of Africa, and a cold front over central and northern Europe. Wind flows from North America are diverging because of the low-pressure system at 50°W; strong winds from the northwest are following the cold front over Europe. Flow aloft over the Atlantic is still zonal. Precipitation (Figure 6b) associated with cold fronts is present in the eastern North Atlantic, central and northern Europe; precipitation is also present around the low-pressure system at 50°W. In the subtropical areas, precipitation is more widespread than on October 15. Eastern North America, under the influence of a high-pressure system, is free from precipitation, except for an area off the eastern coast of Florida and small areas over Nova Scotia and northern Ontario, where a weak low-pressure system is located.

Plate 2 presents plots of the sulfate concentrations at the lowest model level, from the surface to approximately 65 m, for the two selected time periods. As might be expected, concentrations are highest over source regions of Europe and Eastern North America. On October 15 (Plate 2a) the highest concentrations are over eastern Europe. Strong southwest flows over eastern North America and precipitation off the coast have reduced concentrations for these areas and transported emissions from source areas to the north and northeast. Driven by the westerly flow east of Nova Scotia and Newfoundland, concentrations in these areas are higher than in surrounding oceanic areas. The precipitation in the North Atlantic midlatitudes, shown in Figure 5b, has created a corresponding area of low concentrations. In contrast, on October 22 (Plate 2b) the highest concentrations are over eastern North America and the adjacent western North Atlantic, where weak flows prevail and there is no precipitation; the advection of clean maritime air and precipitation have resulted in low concentrations over central

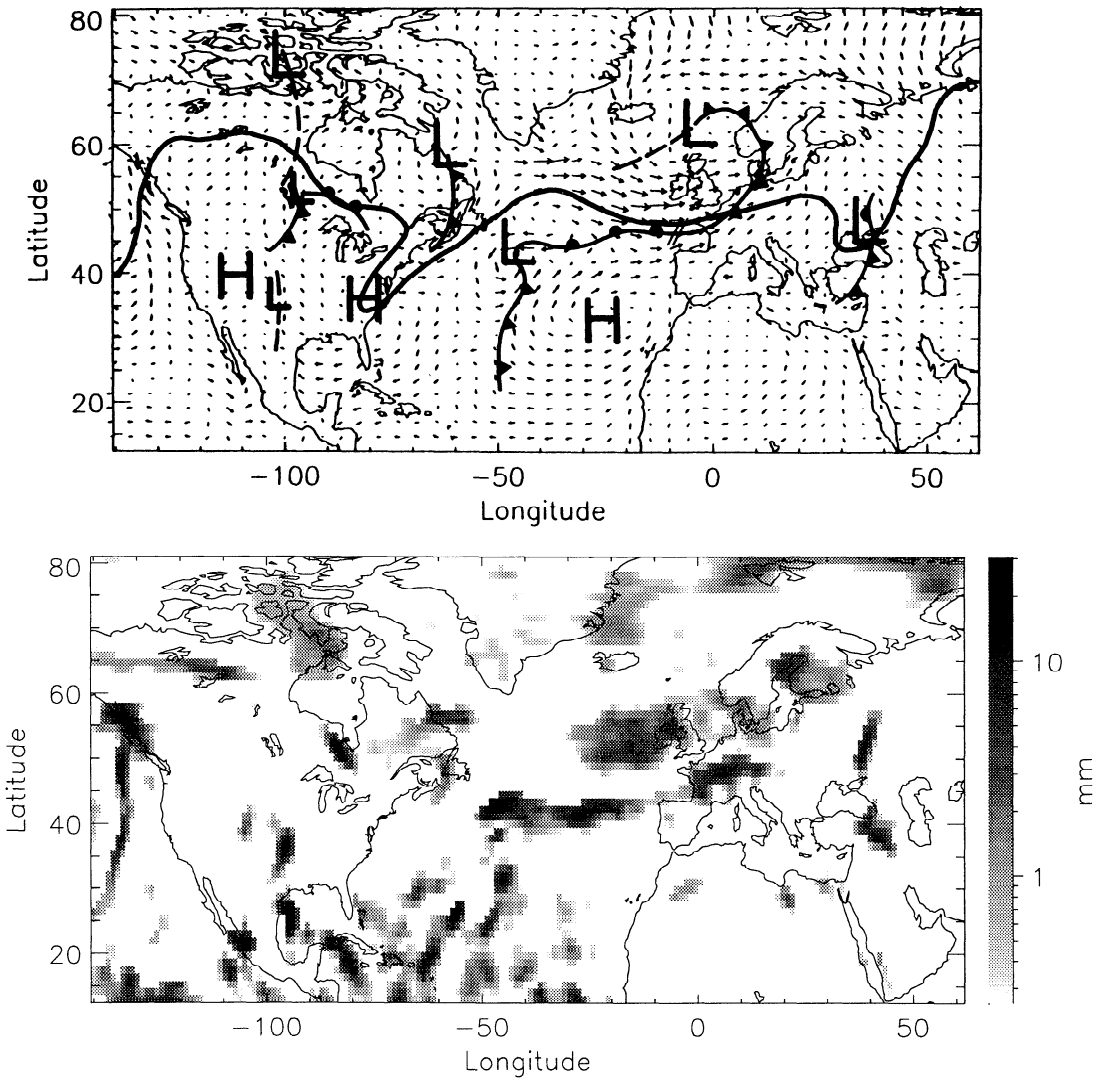

Figure 6. Weather maps for October 22, 1986, 0000 UT. (a) Surface wind vectors and synoptic weather. Solid lines are constant height lines for the 5500-gpm surface. (b) Precipitation amounts in previous 6 hours.

and northern Europe. Areas east of Nova Scotia and Newfoundland, which had exhibited high concentrations on October 15, now exhibit low concentrations. Concentrations over oceanic subtropical regions subject to precipitation are lower than over regions where there has been no precipitation.

The vertical distribution of sulfate concentrations can be examined by means of vertical profiles as a function of latitude at selected longitudes. The meridional section on October 15 at 0600 UT at 40.5°W (Figure 7a; location indicated by the north-south line in Plate 2a) cuts through sections of high surface concentration present over the central Atlantic Ocean. In the area of high surface concentrations between 40°N and 50°N, the highest concentrations are around the 800-hPa level. We observed the development of this area of high concentrations by examining vertical profiles of the sulfate concentrations for the previous 48 hours. On October 13, the high concentrations were located around 65°W and extended from the surface to approximately 600 hPa. On October 14, the high concentrations were located around 50°W, and became isolated from the surface, extending from about 900 hPa to about 630 hPa. On October 15 (Plate 2a), the high concentrations were located around 40°W, and extended from about 850 hPa to about 780 hPa. Such pockets of high concentration aloft have been observed over the North Atlantic, for example, by *Bridgman et al.* [1988]. The meridional section on October 22 at 0600 UT at 30°E (Figure 7b, location indicated by the north-south line in Plate 2b) includes the areas of high concentration present in northeastern Europe. Again there are areas where concentrations aloft greatly exceed those at ground level, e.g., at 48°N and 58°N (0.9 ppb at 400 hPa versus ~0.1 ppb at the surface); there are also areas where high concentrations extend from the surface to above 600 hPa, e.g., at 65°N.

3.2. Sulfate Burden and Source Attribution

The sulfate column burden is important because it leads directly to assessment of enhanced albedo by direct light scattering [*Charlson et al.*, 1991, 1992]. It is therefore of interest to identify the contributions to this burden according to source regions (NA, Eu) and type (anthropogenic, biogenic). Plates 3 and 4 present the geographic distribution of sulfate column burden for the two study periods (October 15 and October 22). In each figure, the top three panels present the contributions by

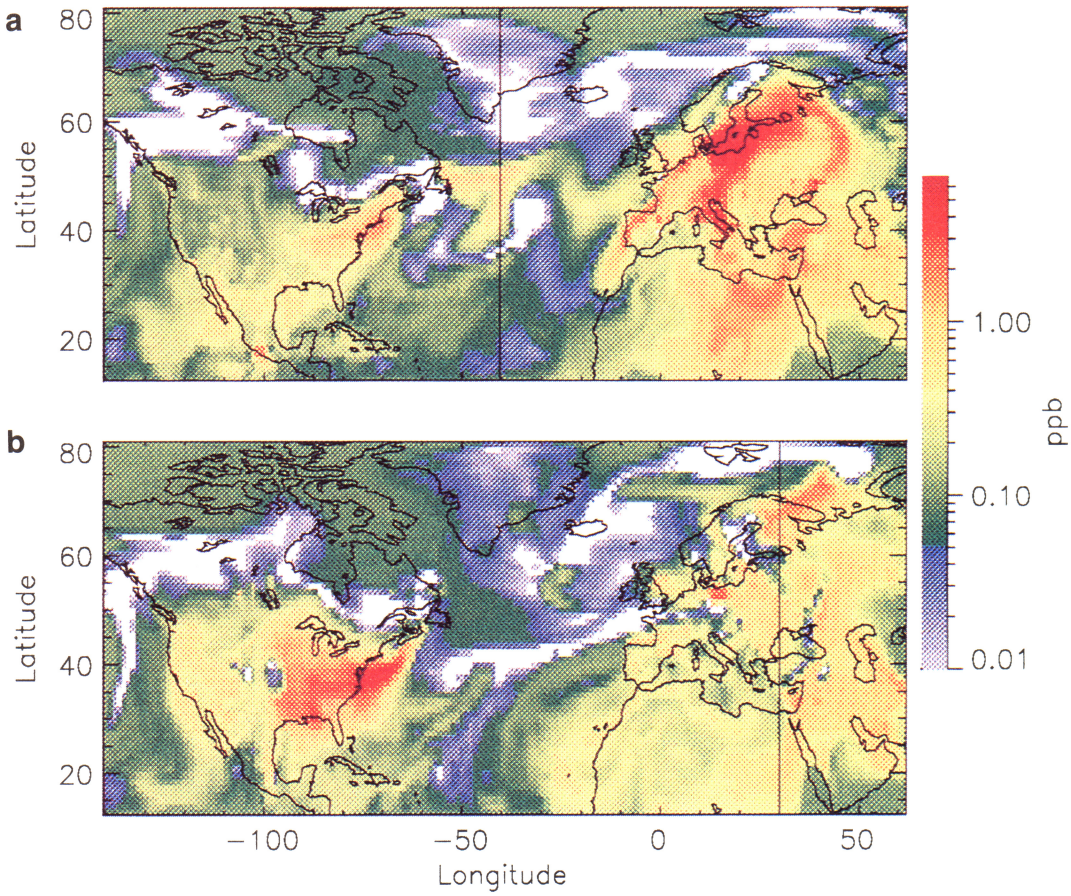

Plate 2. Sulfate concentration at lowest model level (surface to approximately 65 m); 1 ppb is equivalent to 1 nmol sulfate per mole of air. (a) October 15, 1986 at 0600 UT. (b) October 22, 1986, at 0600 UT. White denotes areas with concentrations less than 0.01 ppb. Longitudes of sections used in Figures 7, 40.5°W and 30°E, are indicated in Plate 2a and 2b, respectively.

source region, and the bottom panels present the column burdens from all sources, including the contribution of material transported from outside the model domain. Comparing these maps with the surface concentration maps (Figure 6), we see that the spatial variability of the surface concentration fields is somewhat reduced by the vertical integration performed to compute the column burden; however, the more salient features of the concentrations carry over to the column burdens.

On October 15, the areas of high and low surface concentration between 40°N and 50°N over the Atlantic (Figure 6a) are identifiable in the column burden map (Plate 3d), but the variability over oceanic areas south of ~40°N has been diminished. In contrast, the plume southwest of Mexico City is more prominent in the column burden map, indicative of concentrations aloft exceeding those at the surface. European sources contribute to the column burden mainly over land areas east of 20°W; the major influences of North American sources are in the area around Mexico City, in areas off the eastern coast of North America, and across the Atlantic east of Nova Scotia. The 48-hour development of the area of higher column burdens east of Nova Scotia can be followed by the sequence of Plates 5 and 3d. Strong southwest winds over the northeast coast of North America, and zonal flows across the North Atlantic off the coast of Nova Scotia have transported emissions from the northeastern United States north, so that on October 13 (Plate 5a) high column burdens are located over the U.S.-Canadian border and over Nova Scotia. Twenty-four hours later, on October 14 (Plate 5b), the strong winds have moved off the northeast coast of North America, and material is being transported by the zonal flow east over the ocean. High column burdens are now located over and east of Newfoundland, over Nova Scotia and over the U.S.-Canadian border. After another 24 hours, on October 15 (Plate 3d), following the wind flows depicted in Figure 5a, material continues to be transported by the zonal flow; high column burdens are located over the central North Atlantic.

On October 22 (Plate 4d), areas of high surface concentration over source regions in eastern North America (Figure 6b) are also areas of high column burden; in eastern Europe the column burdens are relatively higher than the surface concentrations. Again the greatest decrease in spatial variability between the surface concentrations and the column burdens occurs in oceanic areas south of ~40°N. On this date the penetration of European sulfate to the North Atlantic was one of the most prominent for the time period modeled, in this case, over areas around 25°W, 50°N, following the flow from central Europe around the low-pressure area located east of Norway (Figure 6a). Central European areas which exhibited high column burden on October 15 now have lower column burden, as a consequence of a cold front (Figure 6a) bringing maritime air and precipitation from the Atlantic Ocean. The influence of European sources is greatest in the eastern and southern parts of the European continent, following flow around the low-pressure system present over

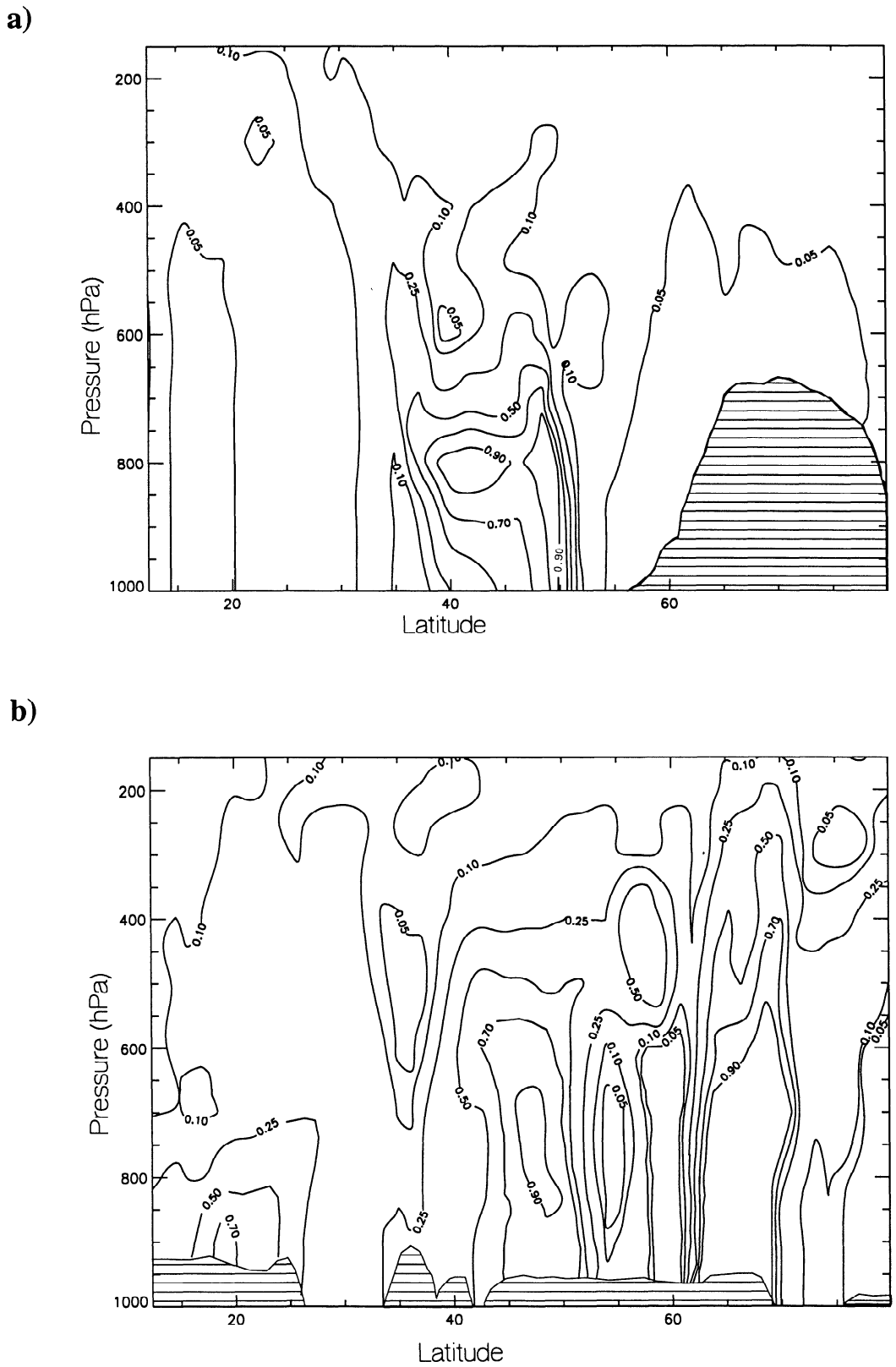

Figure 7. Examples of the vertical distribution with latitude of sulfate concentration for the two study periods. (a) Contours at 40.5°W for October 15, 1986, at 0600 UT, a section that includes areas of high concentrations due to emissions from North American sources. (b) Contours at 30°E for October 22, 1986, at 0600 UT, a section that includes areas of high concentrations due to emissions from European sources. Contour intervals are 0.05, 0.10, 0.25, 0.50, 0.70, and 0.90 ppb.

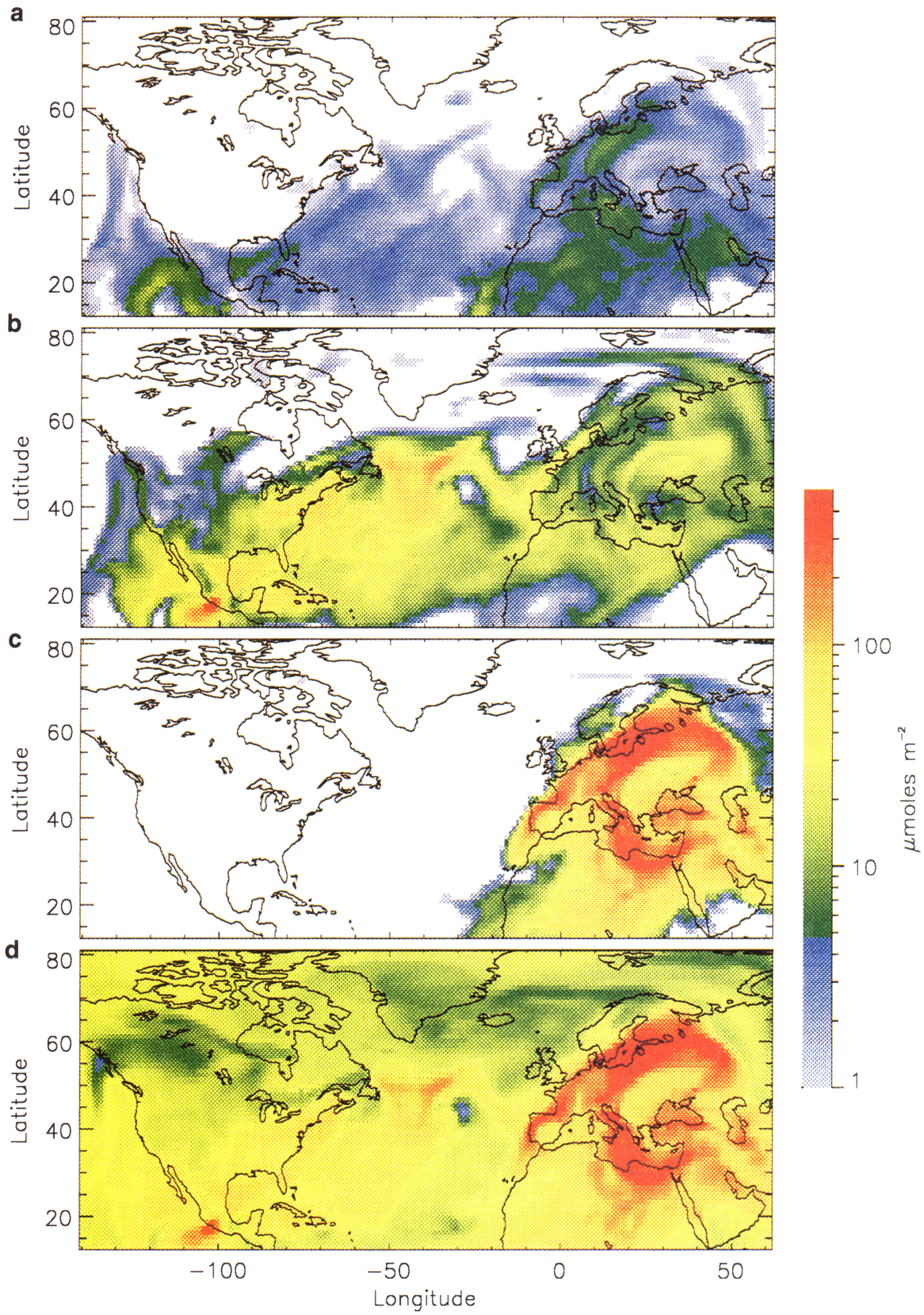

Plate 3. Sulfate column burden for October 15, 1986, at 0600 UT. (a) Burden resulting from bogenic emissions. (b) Burden resulting from North American emissions. (c) Burden resulting from European emissions. (d) Total burden (resulting from emissions above, plus material transported from outside the model domain). White denotes areas with burden less than 1 μmol m^{-2}.

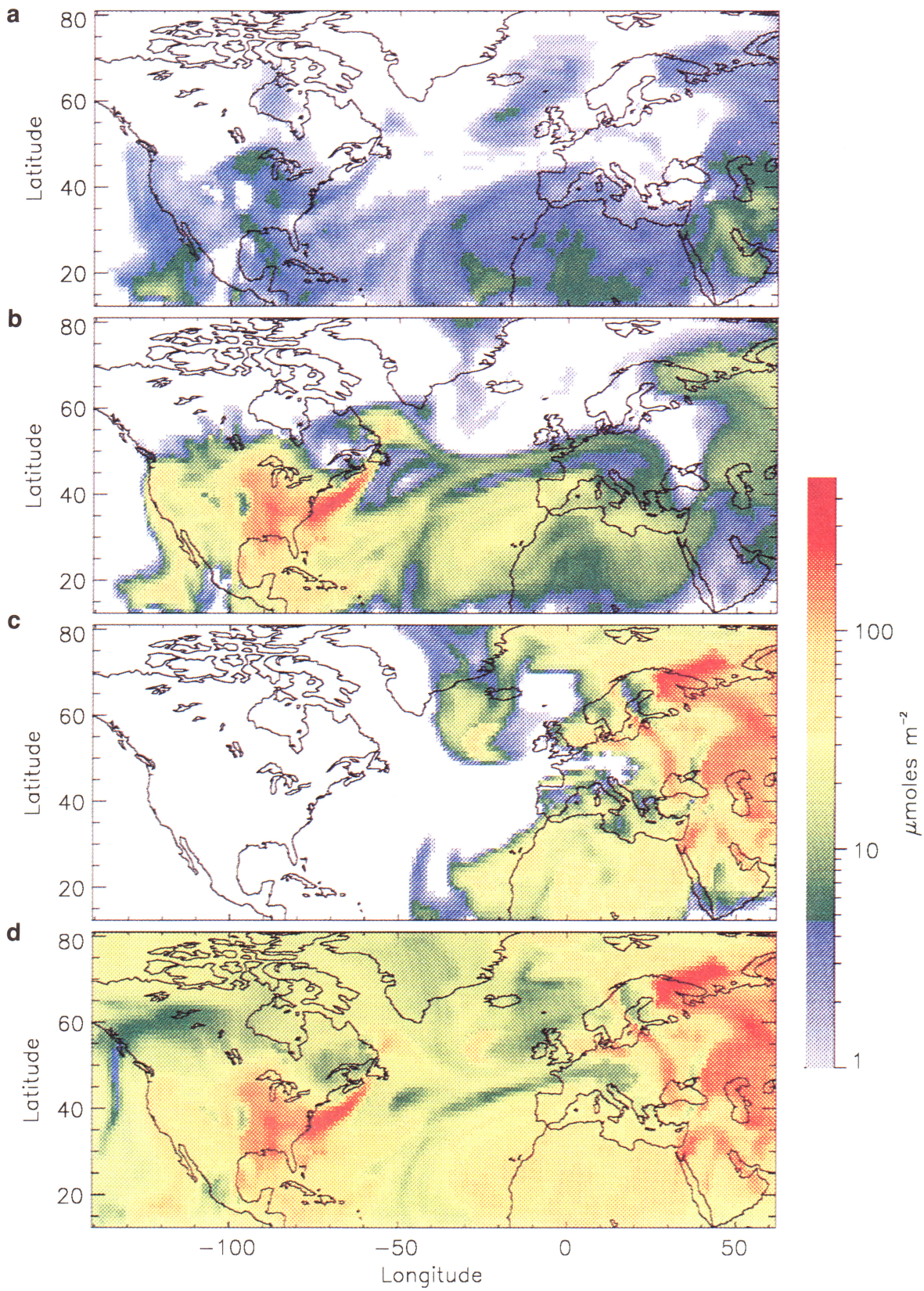

Plate 4. Sulfate column burden for October 22, 1986, 0600 UT. (a) Burden resulting from bogenic emissions. (b) Burden resulting from North American emissions. (c) Burden resulting from European emissions. (d) Total burden (resulting from emissions above, plus material transported from outside the model domain). White denotes areas with burden less than 1 μmol m^{-2}.

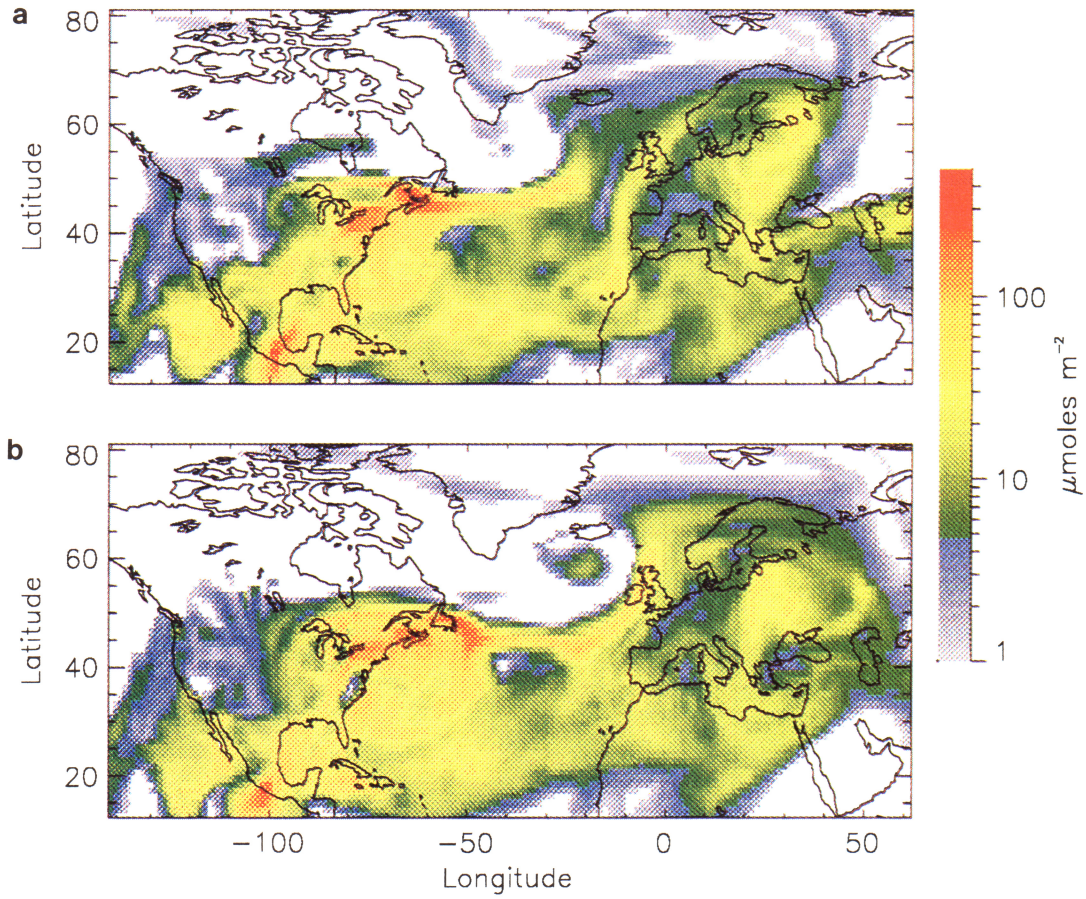

Plate 5. Development of the area of elevated sulfate burden from emissions of North American sources. (a) Sulfate burden on October 13, 1986, 0600 UT. (b) Sulfate burden on October 14, 1986, 0600 UT. Color bar is the same as that used in Plate 3.

eastern Europe and Russia. Because of light winds and the absence of precipitation, the influence of North American sources is strongest just off the east coast over the Atlantic.

To assess the relative contribution of sources to sulfate burdens over broad regions of the model domain, pertinent to addressing the influence of long range transport and the relative influence of anthropogenic and biogenic sources, we calculated the burdens (volume integral of the concentration) for five longitude bands; we then calculated the percent contribution to the burdens resulting from emissions from each of the source types and regions defined in Table 2. Time series of results for the longitude bands are presented in Figure 8. As might be expected, the sulfate burden in the predominantly continental regions (Figures 8a and 8e) is dominated by proximate anthropogenic sources. However, there was a pronounced variability in the magnitude of the relative contributions for the mainly oceanic regions (Figures 8b-8d). North American sources are almost consistently the highest contributors to the sulfate burdens over the mid-North Atlantic (Figure 8c), contributing between 25 and 58% of the burden. European sources contribute between 2 and 33% to the burden in this region; it is seen that the influence of these sources is more pronounced on October 22, at 0600 UT (discussed above), and on November 11 at 0600 UT (not shown), when it exceeds that of North American sources. The high influence of the European sources on October 22 is predominantly north of 50°N (as shown in Plate 4c); on November 11 the high influence of the European sources is predominantly south of 35°N. Biogenic sources contribute between 6 and 12% of the sulfate burden in this region. For certain time periods, North American sources contribute up to 25% of the sulfate burden over western Europe (Figure 8e); for the two study periods (October 15 and October 22), North American sources contribute around 8% of the burden over some areas of western Europe.

Material from outside the model domain makes appreciable contributions to the sulfate burden in each of the five longitude bands of the study area, as demonstrated in Figure 8. This influence is greatest in areas close to the southern and northern borders of the domain; the southern border due to its greater length, and the northern border because these are areas with very low anthropogenic emissions flux, not downwind of source areas during the modeled period, and with very low chemical conversion.

Area-weighted averages by model level demonstrate that in areas away from the boundaries of the domain, the influence of external fluxes is mainly above 8 km and is largely due to influx from the top of the model domain. A flux of sulfate from the stratosphere into the troposphere would be consistent with a stratospheric source, e.g., from oxidation of OCS, and/or SO_2 injected into the stratosphere by intermittent explosive eruptions of volcanoes. Such a source of particles at higher altitudes is postulated by *Han et al.* [1994] based on an analysis of CCN

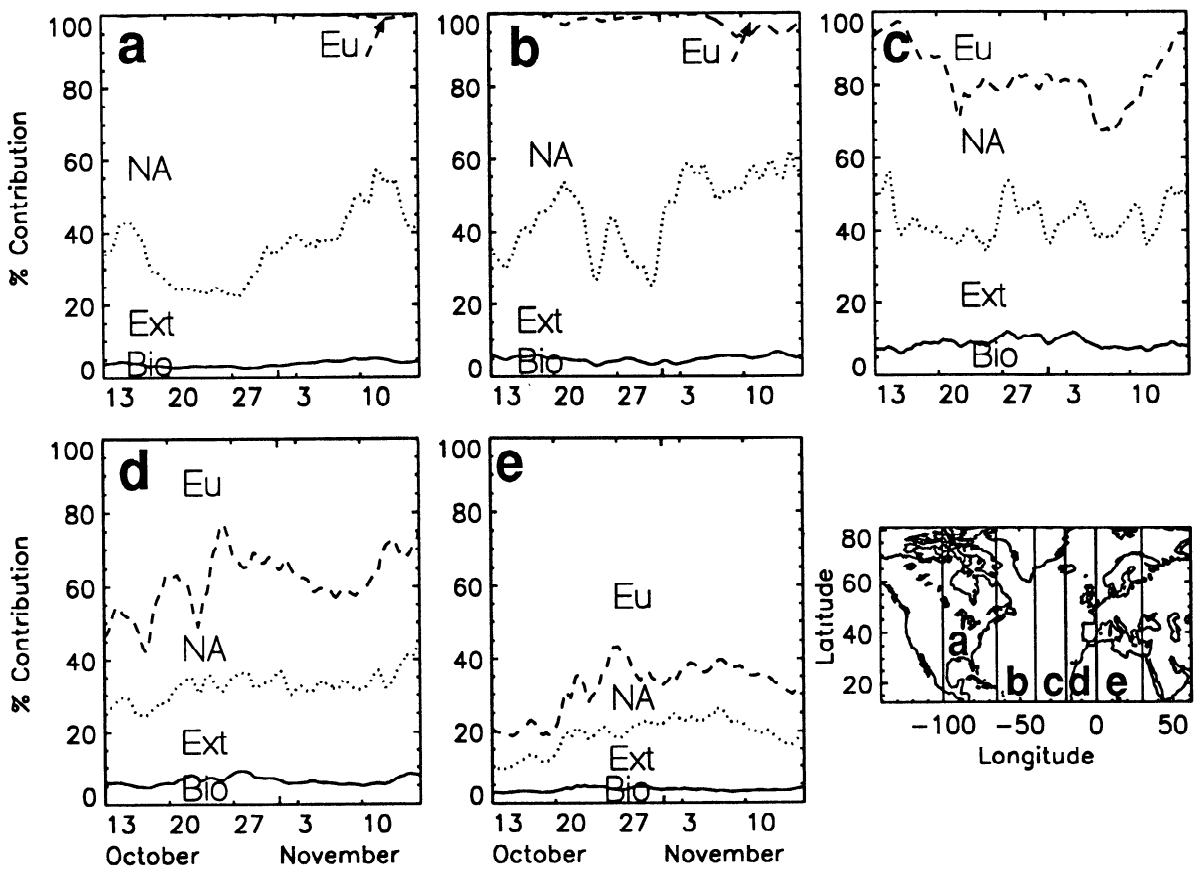

Figure 8. Time series of the percent contribution from each source region to the sulfate burden in five longitude bands: (a) 100°W to 65°W, (b) 65°W to 40°W, (c) 40°W to 20°W, (d) 20°W to 0°, and (e) 0° to 30°E. NA refers to anthropogenic sources west of 30°W; Eu refers to anthropogenic sources east of 30°W, Bio refers to biogenic sources and Ext refers to fluxes external to the model domain.

number and size distribution. The sulfate concentration assumed at the top of the domain, 0.09 ppb, is consistent with the relatively low stratospheric sulfate concentrations in 1986 [*Hofmann*, 1990]; the stratospheric contribution would be considerably greater in the post-Pinatubo era.

Because prevailing wind patterns favor flow into the domain from the western and southern boundaries, and out of the domain from the eastern and northern boundaries, we selected the western and southern boundaries of the domain for this study to be in areas where background concentrations are expected to be dominant. However, background concentrations are not appropriate representations of conditions over continental areas of the eastern boundary of the domain. Moreover, the model domain cannot accurately represent anthropogenic sulfate reentering from the west during meteorological conditions giving rise to recirculation off the west coast of North America, nor the effect of episodic aerosol loadings over the Pacific Ocean, due to emissions in Asia, reported by *Durkee et al.* [1991]. These conditions must be captured in the model if we are to accurately represent sulfate burdens for specific times and locations.

3.3. Process Attribution

It is also possible to examine the contribution of sulfate formed by gaseous and aqueous phase oxidation, and of primary sulfate, since these are computed as separate species in the model. Plate 6 presents this attribution of the sulfate burden from emissions in the model domain on October 15 at 0600 UT. Gas phase generated sulfate is the predominant contributor to the area of elevated sulfate burden over the North Atlantic and to the areas of higher burden over eastern Europe experienced on this date. Sulfate generated by previous precipitation events is the predominant contributor to the plume southwest of Mexico City. We also note the substantial contribution of primary sulfate to the burden over the Baltic Sea. For this date, contributions to the sulfate burden from emissions in the domain were 46% for gas phase generated sulfate, 48% for aqueous phase generated sulfate, and 6% for sulfate from primary emissions. For the entire simulation period, primary sulfate contributes between 5 and 10% of the sulfate burden from emissions in the domain, gas phase generated sulfate contributes between 39 and 54%, and aqueous phase generated sulfate contributes between 37 and 55%.

4. Discussion

4.1. Comparison of Model and Observations

In order to assess the accuracy of the model-predicted sulfate concentrations, we compared daily average model-generated sulfate concentrations at the lowest model level with surface observations from air quality monitoring stations. Data for the monitoring network run by EMEP [*Schaug et al.*, 1988, 1989], which covers western and central Europe, were obtained from the Norwegian Institute for Air Research; data from the Canadian monitoring network were obtained from Environment Canada

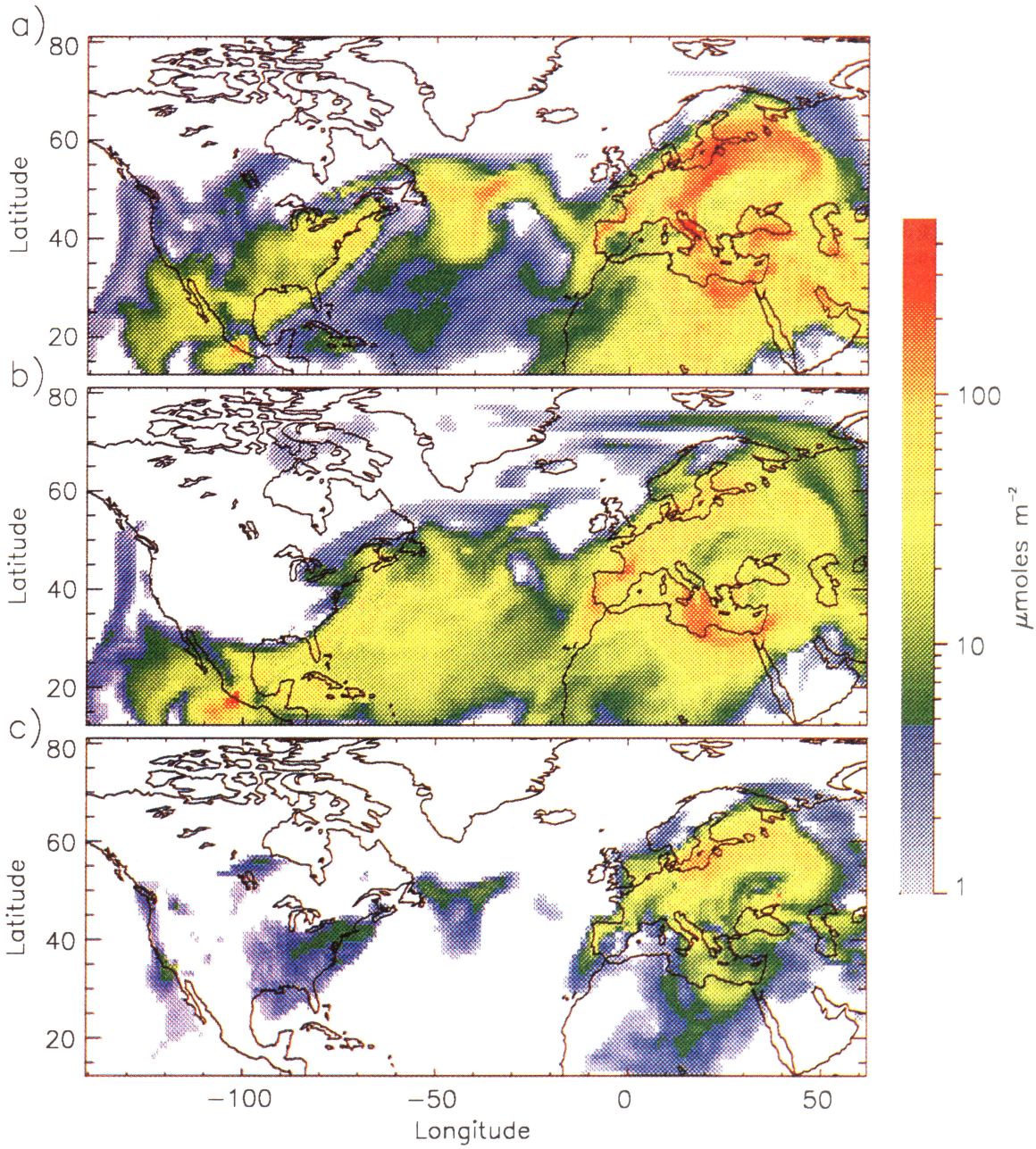

Plate 6. Contributions of sulfate produced by different mechanisms to column burden on October 15, 1986, at 0600 UT. (a) From gas phase generated sulfate. (b) From aqueous phase generated sulfate. (c) From primary sulfate emissions.

(R. Vet, Atmospheric Environment Services, Toronto, Canada, personal communication, 1992). Both networks measure sulfate concentrations daily using 24-hour filter samples. U.S. data were obtained from the Aerometric Information Retrieval System of the U.S. Environmental Protection Agency [*U.S. EPA*, 1988], which includes routine monitoring data from the National Air Monitoring Stations and the State and Local Air Monitoring Stations. The stations measure sulfate using 24-hour glass fiber filter samples once every 6 days. Because the primary purpose of monitoring networks in the United States is to assess population exposure, the majority of these stations are located in urban and suburban settings, and thus tend to be influenced by local pollution sources. Results from high-volume sampling using glass fiber filters exhibit an offset relative to comparable measurements using Teflon filters of approximately 0.89 ppb, possibly because of filter artifacts [*Lipfert*, 1994]; we have subtracted this bias from the data for the U.S. networks, with observations less than 0.89 ppb considered to be below the detection limit. Data were also obtained from stations located in Miami, Florida and Barbados (J. Prospero, University of Miami, Miami, Florida, personal communication, 1993). These stations generally sampled on a daily basis with samplers active only for oceanic wind directions; data were included in our comparisons when the sampling period spanned at least 18 and no more than 28 hours. Daily observations from a station run by the New York State Department of Health at Mayville, New York [*Husain and*

Dutkiewicz, 1990] (L. Husain, New York State Department of Health, Albany, personal communication, 1993), were also included.

To carry out the comparison, the monitoring stations were assigned to their corresponding model grid cell, and 24-hour averages of the modeled sulfate concentrations were calculated for each cell on each day for which observations were available. There were a total of 1733 observations; 70.2% from European stations, 15.4% from Canadian stations, 10.6% from the national and state networks in the United States, 2.0% from the stations at Barbados and Miami, and 1.8% from the station at Mayville, New York. Approximately 44% of model results were within a factor of 2 of the observations, ranging from 42% for European stations to 62% for the Miami and Barbados stations; approximately 66% were within a factor of 3, ranging from 64% for European stations to 85% for the Miami and Barbados stations. Figure 9 presents the distribution of the differences between modeled and observed surface concentrations. The model tends to underpredict the concentrations; the high peak at the center of the distribution is influenced by data from stations located in regions of low concentrations. For observations between 0.5 and 1.0 ppb, 83.1% of the model results are within 0.5 ppb of the observations; for observations between 1.0 and 5.0 ppb, 59.2% of the model results are within 1 ppb of the observations. Table 5 summarizes the modeled to observed surface concentration ratios. Median values for the ratio of the modeled to observed concentrations decrease as the observed concentrations increase, indicating that the model underpredicts more frequently for higher concentrations, perhaps because such high observations are influenced by local sources.

Table 5. Mean, Median, and 10th and 90th Percentiles of the Model/Observed Ratio, and Fraction of Cases Classified by Range of Observed Values

Observed Concentration, ppb	Modeled to Observed Concentration Ratio				
	% Cases	10th Percentile	Median	Mean	90th Percentile
< 0.5	26.5	0.16	0.63	1.2	2.7
0.5 to 1	36.5	0.16	0.54	0.85	1.8
1 to 5	34.0	0.14	0.47	0.58	1.1
5 to 10	2.2	0.11	0.32	0.37	0.71
> 10 (Only three cases)					

Figure 10 presents time series of the observed and modeled surface concentrations at monitoring sites where observational data were available for at least 25 of the 34 modeled days; 43 stations met this criterion. The model accurately reflects the spatial distribution of sulfate concentrations; that is, in almost all cases the stations with low observed concentrations have low modeled concentrations, and those with high observed concentrations have high modeled concentration. There are several instances of remarkably good quantitative agreement in the time series, for example, stations 15, 18, 36, 37 and 41. Even in instances where quantitative agreement was not so close, the episodicity of the concentrations is well represented; that is, the model concentrations track the changes with time in the observed concentrations, for example, at stations 26, 27, 30 and 39. Only stations 10, 11, 12, 25, 32 and 38 exhibited nonsignificant (F-test

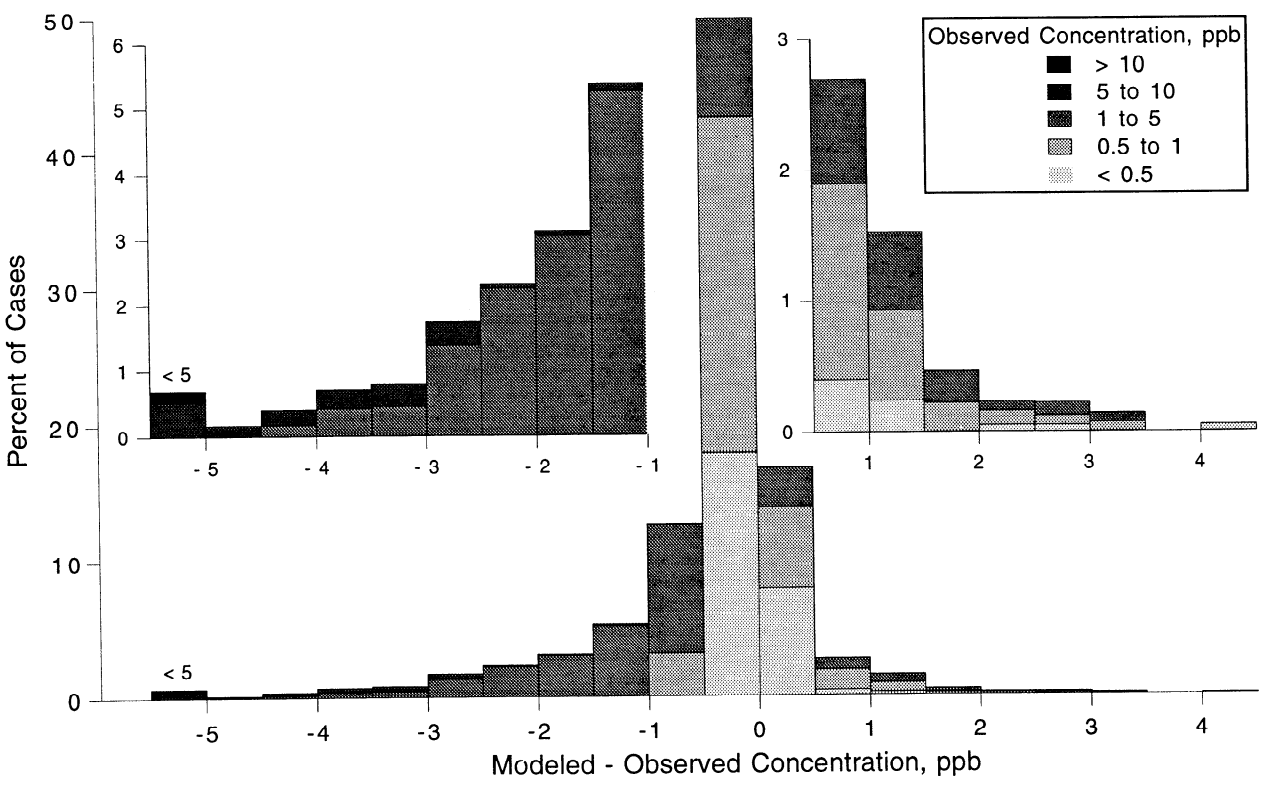

Figure 9. Histogram of (model-observed) values of surface concentrations for all observations of monitoring stations in the United States, Canada, Europe, and Barbados. Comparisons are classified by the observed concentration; inserts expand the scale of the histogram tails.

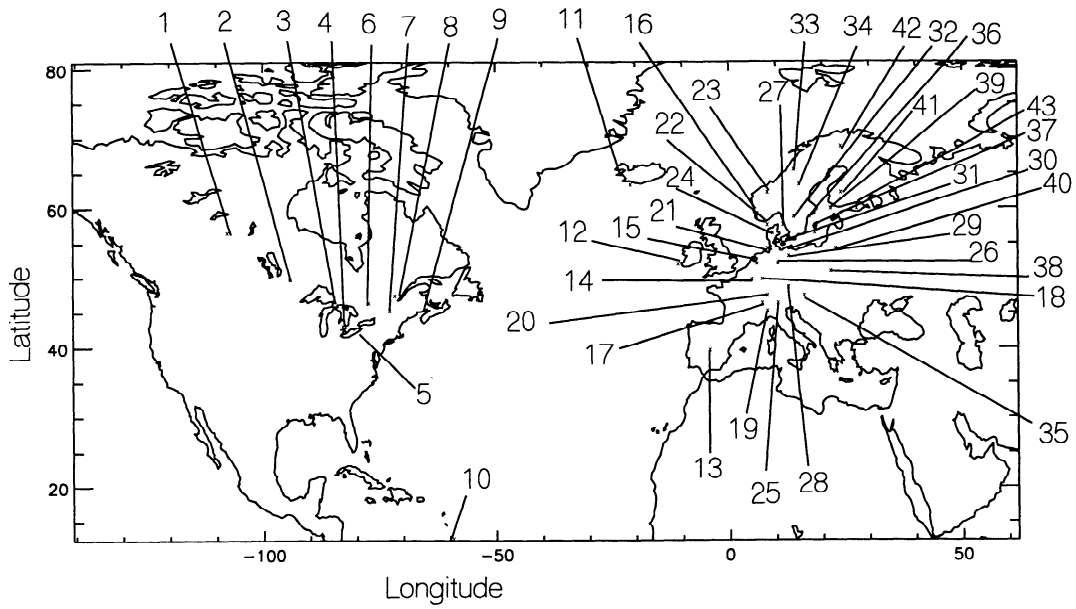

Figure 10a. Locations of monitoring stations with at least 25 observations for the period October 13 to November 15, 1986.

null-hypothesis probability >5%) linear regressions ($y = a + bx$) of the modeled concentrations (y) versus the observed concentrations (x). Station 10 is located in Barbados, at the southern boundary of the model domain, where model concentrations are greatly influenced by the assumed external concentrations. Stations 11 and 12 are coastal stations, where the observed sulfate concentrations could include contributions by sea salt. Stations 25 and 32 are mountain locations, where observed concentrations may not be broadly representative because of local terrain effects. Station 38 is located directly downwind of an area of high anthropogenic emissions, as seen in Plate 1a, where observed concentrations can be influenced by local pollution. For the 37 stations with significant linear regressions, values of the slope ranged from 0.13 to 1.18; only one value was greater than 1.

Model results and observations for wet deposition of sulfate were also compared. Wet deposition data (sulfate concentration multiplied by precipitation) for several networks in North America were obtained from the acid deposition system (E. Bittner, Battelle Pacific Northwest Laboratories, Richland, Washington, personal communication, 1990) [*Watson and Olsen*, 1984]. The networks monitor wet deposition on a weekly basis. The modeled sulfate depositions were aggregated to correspond with the time periods monitored by each station, and results were compared. These comparisons include the effects of both the wet removal processes in the model and the precipitation amounts in the meteorological data set; an evaluation of the precipitation is presented in Appendix A. There were a total of 500 measurements of wet-deposited sulfate during the modeled period; the model predicted the occurrence of precipitation for 81.2% of these measurements. The median value of the model/observed ratio for this subset was 0.85; 61% of the model wet deposition results were within a factor of 3 of the observations.

As with the precipitation testing described in Appendix A, there are problems with the representativeness of both the surface concentration and the wet deposition data sets. In all but one case, cell averages for the observations in both data sets were based on a single monitoring station; thus, cell-average results from the model are being compared with point observations within the corresponding cell. In addition, the wet deposition comparison is affected by the fact that precipitation events at observing stations do not start or end within the 6-hour time increment of the meteorological data, so discrepancies may also occur in aggregation of the modeled data.

These comparisons show that the model results are generally lower than the observations for both sulfate surface concentration and wet deposition. Further, model underpredictions occur mostly at peak values of the observed concentrations, and for stations located in high emissions areas; in contrast, overpredictions occur mostly when observed concentrations exhibit abrupt decreases and, for some time periods, at locations in the vicinity of areas of high emissions. This behavior indicates that the model may be underestimating sulfate generation, and that sulfate removal in the model is affected by uncertainties in the location and amount of precipitation. A major source of underestimation of sulfate may be the lack of representation of aqueous phase conversion in nonprecipitating clouds. We note that in a recent modification to RADM [*Dennis et al.*, 1993], the best correction for the underprediction of ambient sulfate by that model was provided by refinements to the treatment of reactions in nonprecipitating cumulus clouds.

Our model is perhaps most comparable to that of *Tarrason and Iversen* [1992], who estimated the contribution of North American emissions to the monthly average particulate sulfate surface concentrations and the monthly wet deposition at 15 grid points along the western land points of Europe for October 1982, and January, April, and July 1983. These investigators estimated monthly average particulate sulfate surface concentrations due to North American sources between 0.008 and 0.1 ppb, with the highest values in the October 1982 and July 1983 simulations. Estimates of the contribution of these sources to monthly wet deposition were less than 0.4 mmol S m^{-2}, with the highest values in the January 1983 simulation. For the northernmost 14 grid points listed by Tarrason and Iversen, we estimate the North American contribution to be from 0.002 to 0.06 ppb for the

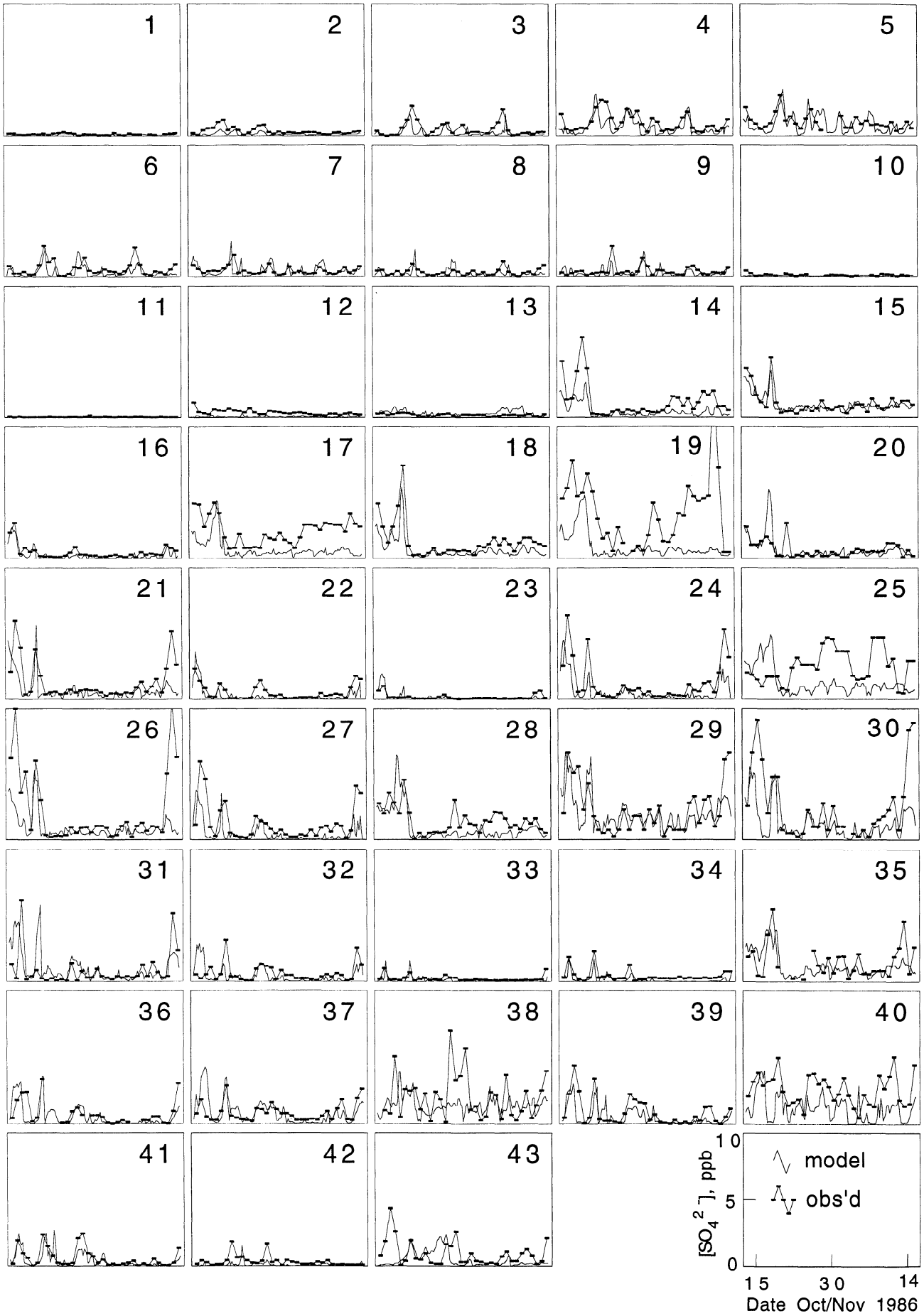

Figure 10b. Time series of modeled and observed values for surface concentrations at stations with at least 25 observations for the period October 13 to November 15, 1986.

monthly averaged particulate sulfate surface concentrations and from 0.04 to 0.5 mmol S m^{-2} for the monthly wet deposition. Compared to the Tarrason and Iversen October 1982 simulation, the current model estimates lower values for the sulfate air concentrations and higher values for the wet deposition. The extent to which differences in concentrations and deposition are due to differences in meteorological conditions for October 1982 and October 1986, and to differences in the model parameterizations of the chemical mechanisms and wet removal cannot be determined.

4.2. Sinks, Yields, and Turnover Times

Quantities such as yield and turnover time for both SO_2 and sulfate, derived from model simulations, are of interest to assess performance of the model relative to other estimates of these quantities, and for use in box models, such as those estimating sulfate radiative forcing [*Charlson et al.*, 1990, 1992]. The present model results do not represent a steady state system; in addition, the model domain is not "closed", i.e., material flows out of the horizontal and top boundaries (flow into the model domain has been treated as separate species); consequently, evaluation of the quantities of interest can be confounded by these fluxes, necessitating care in the specification of sources and sinks [*Schwartz*, 1979]. Evaluation of quantities such as yield and turnover times based on ratios of reaction and deposition rates and burdens to source rates will result in underestimates, since the amount of material in the model domain will be reduced not just by the processes of concern, but also by the transport of material out of the domain. On the other hand, using sink rates in these calculations does not suffer from this bias, because flow out of the model domain diminishes the amount of material in the domain and the sink rates in roughly the same proportion. For SO_2 the total sink rate, S, including only physical and chemical processes (i.e., not including material transported out of the model domain) is

$$S_{SO_2} = C_{SO_2} + D_{SO_2} + W_{SO_2}$$

where C is the rate of chemical conversion, D is the dry deposition rate, and W is the wet removal rate, all summed over the model domain. Similarly, for sulfate the sink is the sum of the dry deposition and wet removal,

$$S_{SO_4^{2-}} = D_{SO_4^{2-}} + W_{SO_4^{2-}}$$

With these definitions we obtain an unbiased estimate of the sulfate yield (fraction of SO_2 oxidized to sulfate in the atmosphere) as

$$y_{SO_4^{2-}} = C_{SO_2}/S_{SO_2}$$

Similarly, the MSA yield from DMS can be evaluated as

$$y_{MSA} = C_{DMS}/S_{DMS}$$

We calculated sulfate yield from SO_2 and MSA yield from DMS, using 24-hour moving averages. Figure 11a presents a time series of the total sulfate yield. The most important influence in the temporal variability of the sulfate yield is the variability of the aqueous phase conversion, which is driven by the variability in the frequency of occurrence of precipitation; in addition, there is a slow decrease in the OH concentrations over the time period modeled due to the change in the solar zenith angle. Table 6 presents the average sulfate and MSA yields

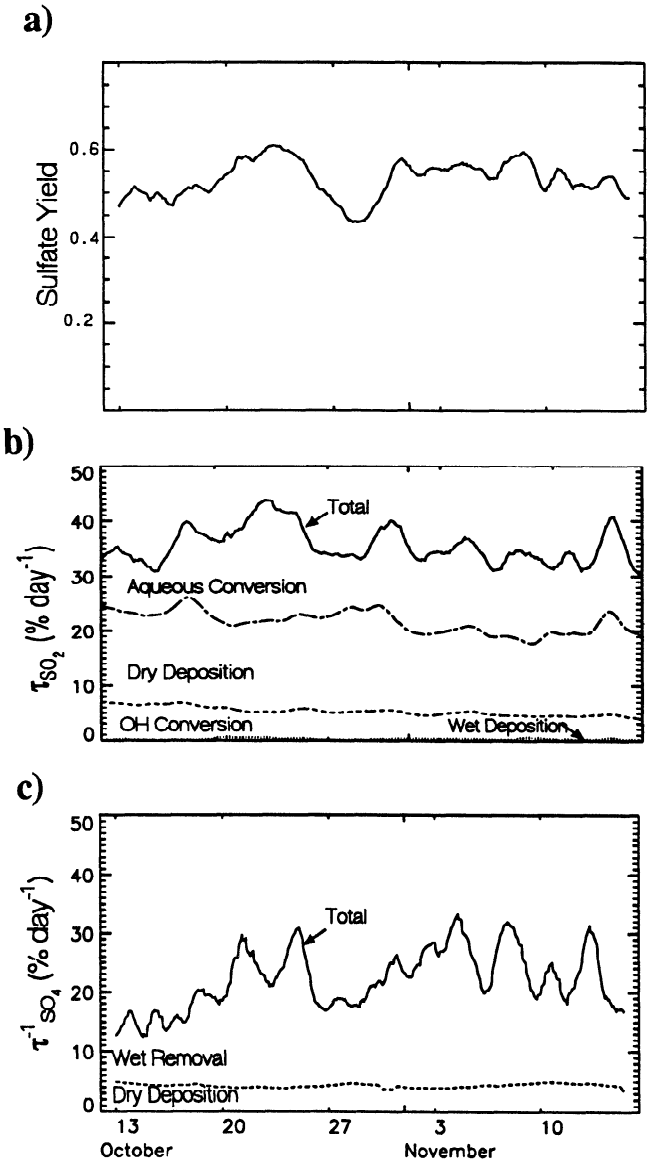

Figure 11. (a) Total sulfate yield (fraction of SO_2 that is oxidized to sulfate). (b) Effective first-order removal rate (τ^{-1}) for SO_2, showing the cumulative contributions to removal by wet deposition, gas phase (OH) conversion, dry deposition, and aqueous phase conversion. (c) The τ^{-1} for sulfate, showing the cumulative contribution to removal by dry deposition and wet deposition.

according to source type and region. These results are comparable to those of other investigators. *Rodhe and Isaksen* [1980] obtained a global yield of almost 50%, *Langner and Rodhe* [1991] obtained sulfate yields in the northern hemisphere ranging from 34 to 48% (depending on the in-cloud oxidation rate used), and *Charlson et al.* [1992] used a global mean of 40% in their box model calculations.

An unbiased estimate of the turnover time (mean residence time), τ, for any species is given as

$$\tau = B/S$$

where B is the burden (moles) in the domain. The inverse of this quantity, τ^{-1}, can be considered an effective first-order removal

Table 6. Sulfate Yield (Fraction of SO_2 Oxidized to Aerosol Sulfate), MSA Yield (Fraction of DMS Oxidized to MSA) and Turnover Times (τ) for Sulfate and MSA

	Source				
	All Sulfate	N. American Sulfate	European Sulfate	Biogenic Sulfate	Biogenic MSA
Yield, %	53 (4)	60 (6)	47 (6)	72 (2)	13 (1)
τ^{-1}, % d^{-1}					
Dry deposition	4.3 (0.3)	3.6 (0.5)	4.8 (0.6)	2.8 (0.2)	3.0 (0.1)
Wet deposition	17.9 (5.1)	21.8 (9.4)	16.5 (5.2)	9.1 (1.8)	18.6 (2.5)
Total	22.2	25.4	21.2	11.9	21.1
τ, days	4.7 (1.1)	4.4 (1.4)	5.0 (1.4)	8.6 (1.3)	4.8 (0.6)

Here, τ^{-1} is the effective first-order removal rate for the different sinks of aerosol sulfate and MSA. Quantities in parentheses are standard deviations.

rate of a species; τ^{-1} for the different sinks of a species are additive.

The average τ^{-1} for each removal process and the total τ^{-1} are shown in Table 6 for aerosol sulfate (taken here as the sum of species ${}^{s}SO_4^{2-}$ and ${}^{p}SO_4^{2-}$) and in Table 7 for SO_2; time series of the total values are plotted in Figure 11b and 11c. Note the larger standard deviations in τ^{-1} of the wet deposition sink for sulfate (~30%) and in the aqueous phase conversion of SO_2 (~22%) than in other τ^{-1} values, indicative of the variability in the frequency of occurrence of precipitation, even when averaged over a large domain.

The τ^{-1} values for the wet and dry deposition sinks of biogenic sulfate (Table 6) are less than the corresponding values for these quantities for anthropogenic sulfate. The τ^{-1} value for the aqueous phase conversion of biogenic SO_2 (Table 7) is higher than the corresponding value for this quantity for anthropogenic SO_2. A possible explanation for these difference may be the different geographic and vertical distributions of the material from the two sources. Anthropogenic emissions (Plate 1a) are concentrated in the midlatitudes, whereas biogenic emissions (Plate 1b) are greatest in the subtropical areas of the domain. The time integral of the precipitation (Figure 12a) shows that these subtropical areas have higher precipitation west of 30°W, and very low precipitation east of 30°W. The lower SO_2 concentrations in areas where biogenic sources prevail, which are areas of higher precipitation, allow aqueous phase conversion to be active and H_2O_2 can process a greater fraction of the biogenic SO_2, resulting in higher sulfate yield. In contrast, aerosol sulfate from biogenic sources is located predominantly over arid land areas east of 30°W, as seen in Figure 12b, which presents the volume- and time-integrated sulfate burden from biogenic sources; these areas have lower wet deposition rates. The lower dry deposition τ^{-1} for the sulfate aerosol from biogenic sources is influenced by the differences in the fractional amounts of material in the lowest model level (and thus subject to dry deposition); area-weighted averages are 2.2% for anthropogenic sulfate and 1.4% for biogenic sulfate.

Overall, the major sink for sulfate is wet deposition. Average contributions to the sinks of aerosol sulfate, derived from Table 6, are 22% from dry deposition and 78% from wet deposition. These results are comparable to the global averages from the Rodhe and Isaksen model, where dry deposition accounted for 25% and wet removal accounted for 75% of sulfate sinks, and to those of Langner and Rodhe, who obtained northern hemisphere contributions to sulfate sinks of 16% for dry deposition and 84% for wet removal.

The turnover time for anthropogenic sulfate, 4.7 ± 1.1 days in Table 6, is comparable to previous estimates. Turnover times of 5 to 10 days have been inferred from measurements of atmospheric concentrations of natural and bomb-test radioactive species, which can be considered surrogates for accumulation-mode aerosol particles [*Junge*, 1963; *Chamberlain*, 1991]; and turnover times of 7 to 9 days were inferred from the decay of atmospheric concentrations of aerosol ^{137}Cs in the weeks following the Chernobyl accident [*Cambray et al.*, 1987]. Results are also quite comparable to overall sulfate turnover times obtained from previous models. *Slinn* [1983] used a 2-km-high box model with dry and wet deposition velocities derived from particle size considerations to estimate turnover times for sulfate particles of about 6 days. *Rodhe and Isaksen* [1980]

Table 7. Turnover times (τ) for SO_2 and DMS

	Source				
	All SO_2	N. American SO_2	European SO_2	Biogenic SO_2	Biogenic DMS
τ^{-1}, % d^{-1}					
Dry deposition	16.4 (1.5)	14.7 (2.2)	17.4 (1.5)	13.3 (0.9)	
Wet deposition	0.29 (0.13)	0.29 (0.22)	0.30 (0.18)	0.09 (0.05)	
[OH] conversion	5.0 (0.8)	5.5 (1.0)	4.7 (0.8)	6.8 (0.8)	35.3 (5.2)
Aqueous conversion	14.1 (3.1)	17.4 (4.9)	11.5 (3.9)	27.4 (2.6)	
Total	35.7	37.9	33.9	47.6	35.3
τ, days	2.8 (0.2)	2.7 (0.3)	3.0 (0.3)	2.1 (0.2)	2.9 (0.4)

Here, τ^{-1} is the effective first-order removal rate for the different sinks. Quantities in parentheses are standard deviations.

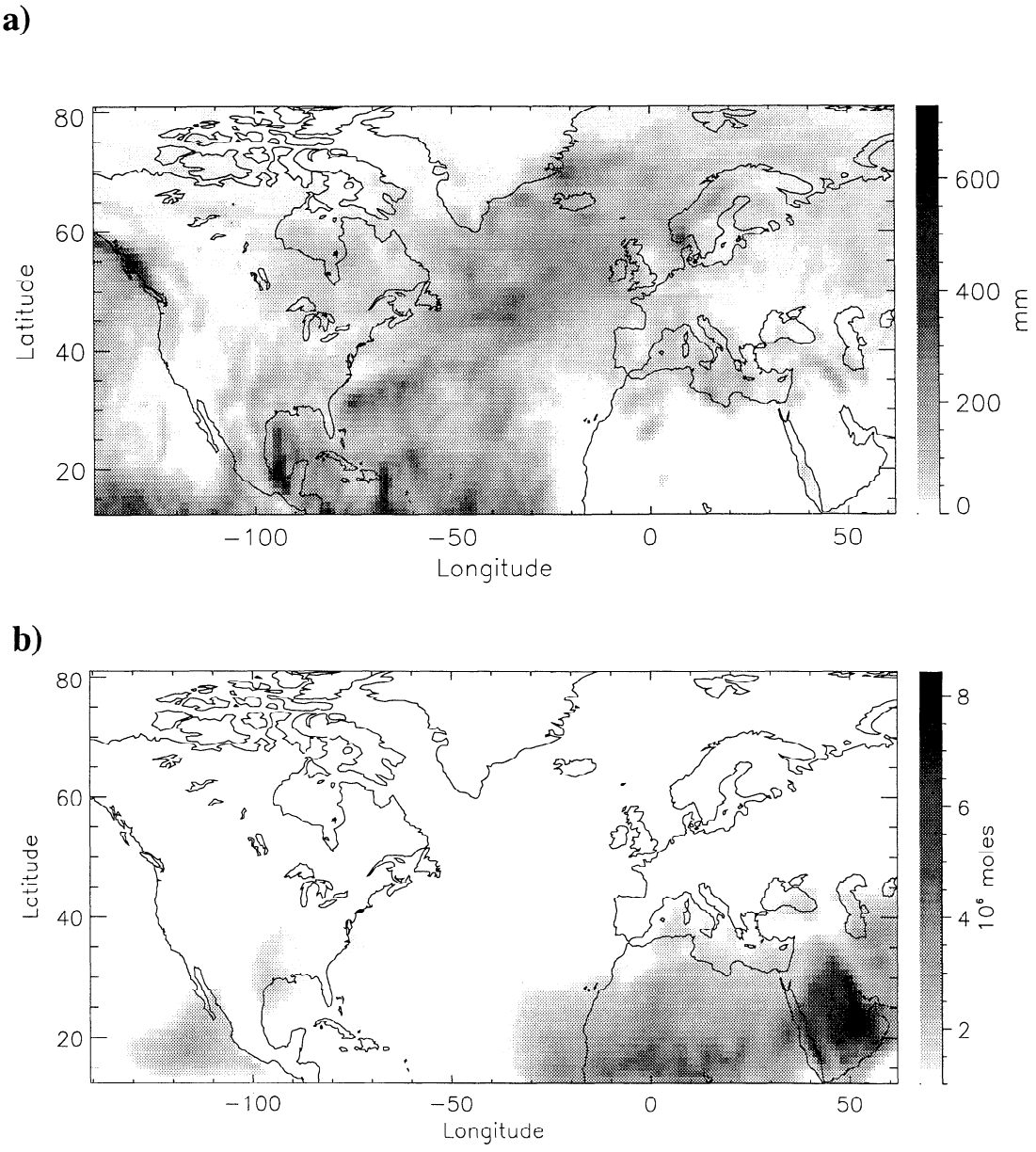

Figure 12. (a) Time integral (over the 34 simulation days) of the precipitation in the model domain. (b) Time integral of the aerosol sulfate burden (volume integral of the concentration) resulting from emissions of biogenic sources.

estimate a turnover time of 4 days for sulfate released up to 3 km. *Langner and Rodhe* [1991] estimate turnover time of approximately 5 days. *Giorgi and Chameides* [1986] show that a species' average lifetime strongly depends on the characteristics of the precipitation regime, and on the release height of the material (for example, surface versus stratospheric sources). Material released in the stratosphere are found to have higher lifetimes than material of surface origin; model simulations show lifetimes of 4, 7, and 13 days for aerosols at 2, 6, and 10 km. It appears that variations in aerosol lifetimes that have been empirically inferred by various investigators can be attributed to different vertical distributions of the aerosol. *Balkanski et al.* [1993] show a dependence of turnover times on the initial release height of the material and on the meteorological conditions encountered. Long turnover times were found when the material was produced at high altitudes, whereas short turnover times were found in areas of high precipitation. Zonal mean turnover times for northern midlatitudes vary from approximately 4 to 6 days in winter, and from approximately 6 to 15 days in summer.

It should be emphasized that sulfate yields and aerosol residence times cannot be considered constants of nature or to have unique values, even over a restricted model domain and period such as the present one. The results of Giorgi and Chameides and of Balkanski et al. clearly address this point, and explain the shorter residence times obtained here compared to those inferred from observations with radionuclides: the sulfate aerosol emanates from surface sources, in comparison, say, with the Chernobyl radionuclides, whose lifetimes were estimated over a 6-week period, and are thus influenced by the material that reached higher levels of the atmosphere.

With respect to the issue of radiative forcing by anthropogenic aerosols, we note that *Charlson et al.* [1991] used a mean residence time of 6 days and *Charlson et al.* [1992] used a mean residence time of 7 days; a turnover time of 4.7 days obtained here, while within the uncertainty of 40% ascribed by those investigators to their estimate of that quantity, would reduce the estimated forcing by approximately 30%. On the other hand, despite the somewhat lower residence time obtained here, there is substantial long-range transport of this aerosol, and substantial enhancement of sulfate burdens over the North Atlantic by North American sulfate, as indicated in Plates 3-5 and Figure 8.

Overall, the major sink for SO_2 is dry deposition. Average contributions to the sinks of SO_2, derived from Table 7, are 46% from dry deposition, 0.6% from wet deposition, 14% from gas phase conversion, and 38% from aqueous phase conversion. These results are in general comparable to the global averages of *Rodhe and Isaksen* [1980], which show contributions to SO_2 sinks in July (January) of 47% (52%) for dry deposition, of 7% (8%) for wet removal, of 21% (12%) for gas phase conversion, and of 18% (23%) for aqueous phase conversion, plus an additional 8% (5%) for the reaction with CH_3O_2, which is no longer considered important [*NASA*, 1991]. The present results are also comparable with those of Langner and Rodhe, who obtained northern hemisphere contributions to SO_2 sinks between 35% and 41% for dry deposition, between 15% and 24% for wet removal, between 8% and 12% for gas phase conversion and between 23% and 42% for aqueous phase conversion, depending on the in-cloud oxidation rate used. The higher wet deposition for SO_2 may be due to the enhanced uptake into the aqueous phase via the formation of the hydroxymethanesulfonate adduct included in this model.

The present results for turnover time (Table 7) for SO_2 and DMS are quite comparable with those of previous investigators; the turnover time for SO_2 may be somewhat high because reactions in nonprecipitating clouds are not represented in the model. *Rodhe and Isaksen* [1980] estimated annual SO_2 turnover times of approximately 1.3 days for releases up to 3 km; *Langner and Rodhe* [1991] obtained annual average turnover times between 1 and 2 days for SO_2 and approximately 3 days for DMS.

4.3. Scales of Temporal and Spatial Variability

To characterize the temporal variability of the sulfate column burden, we examine the autocorrelation coefficient, $\rho(T)$, calculated as

$$\rho(T) = \frac{\int [b(t) - \bar{b}]\,[b(t+T) - \bar{b}]\,dt}{\int [b(t) - \bar{b}]^2\,dt}$$

where T is the lag time, $b(t)$ is the sulfate column burden at time t, and $\bar{b}$ is the average burden over the modeled period. This function decreases from unity (at $T = 0$), to zero at long times. The rate of decrease with increasing T is thus a measure of temporal autocorrelation.

Values of $\rho(T)$ were calculated for each grid cell in a region of the central North Atlantic well away from sources (60°W to 10°W; 30°N to 60°N), and the dependence of $\rho(T)$ on lag time T was examined. The average characteristic time (time for $\rho(T)$ to decrease from 1 to $1/e$) was 10 hours, with 95% of the values being 25.5 hours or less. These results demonstrate a high degree of temporal variability in sulfate column burdens, even in a region well removed from sources, which must be attributed to variations in transport winds and removal rates. This high variability indicates that time resolution of less than 24 hours must be used in order to appropriately capture the temporal pattern of the sulfate concentrations and column burdens.

The high temporal variability of sulfate concentrations and resulting aerosol burdens have been established by observational data. *Husain and Dutkiewicz* [1990] measured sulfate concentrations at Whiteface Mountain, New York, and *Wesely* [1982] measured optical depth on clear, cloudless days for April 1 to October 1 in 1977 and 1978, at 10 stations in eastern North America; in both cases, the observed quantity can change (increase or decrease) by as much as a factor of 10 in 24 hours. This behavior represents a major difference in climate forcing by aerosols, as compared to the forcing by greenhouse gases such as CO_2 and CH_4, which have a much more uniform spatial and temporal distribution; these differences must be appropriately represented in climate models.

To describe the spatial variability of sulfate column burdens, we evaluated variograms of the model results. The definition of a variogram is [*Isaaks and Srivastava*, 1989]

$$\gamma(\mathbf{h}) = \frac{1}{2N(\mathbf{h})} \sum_{(i,j)|\mathbf{h}_{ij}=\mathbf{h}} (b_i - b_j)^2$$

We normalized this quantity to approximately unity at great distances by

$$\gamma_n(\mathbf{h}) = \frac{\gamma(\mathbf{h})}{(1/N)\sum_i (b_i - \bar{b})^2}$$

Here $\gamma(\mathbf{h})$ is the variogram for distance vector $\mathbf{h}$, $\gamma_n(\mathbf{h})$ is the normalized variogram, $N(\mathbf{h})$ is the number of points included in calculations for the distance vector, b_i and b_j are the sulfate column burden at locations i and j along the distance vector, N is the total number of points in the region, and $\bar{b}$ is the average column burden in the region. Values of the normalized variograms increase from 0 (at $\mathbf{h} = 0$) to approximately 1 at large distances.

For the central North Atlantic region the model latitude/longitude grid was projected onto an azimuthal-equidistant grid to obtain great circle distances between the centers of the grid cells. Variograms were calculated at 10° increments and distance increments of 125 km, using routines in the geostatistical library of *Deutsch and Journel* [1992]. The resulting variograms for the two sample times (October 15 at 0600 UT and October 22 at 0600 UT) are presented in Plates 7a and 7b. Plate 7c presents the average of all variograms for the modeled time period. We note that in those figures the expected point symmetry around the origin is broken at large distances because on a sphere $\alpha_{ji} \neq \alpha_{ij} + 180°$, where α_{ij} is the true azimuth of point i with respect to j, but this is of little consequence. The contour at ($1 - 1/e = 0.63$) is drawn to indicate the characteristic autocorrelation distance as a function of azimuth.

For October 15, the minimum characteristic distance is approximately 550 km at 155° (angles are clockwise from north), and the maximum characteristic distance is approximately 1800 km at 35°. For October 22, the minimum is approximately 380 km at 150°, and the maximum is approximately 2000 km at 290°. For the 34-day modeled period, the minimum value of the average characteristic distance is 900 km, with 10th and 90th percentiles values of 400 and 1700 km. These results demonstrate that to capture the spatial variability of the sulfate column burdens, a horizontal grid spacing of approximately 1° is

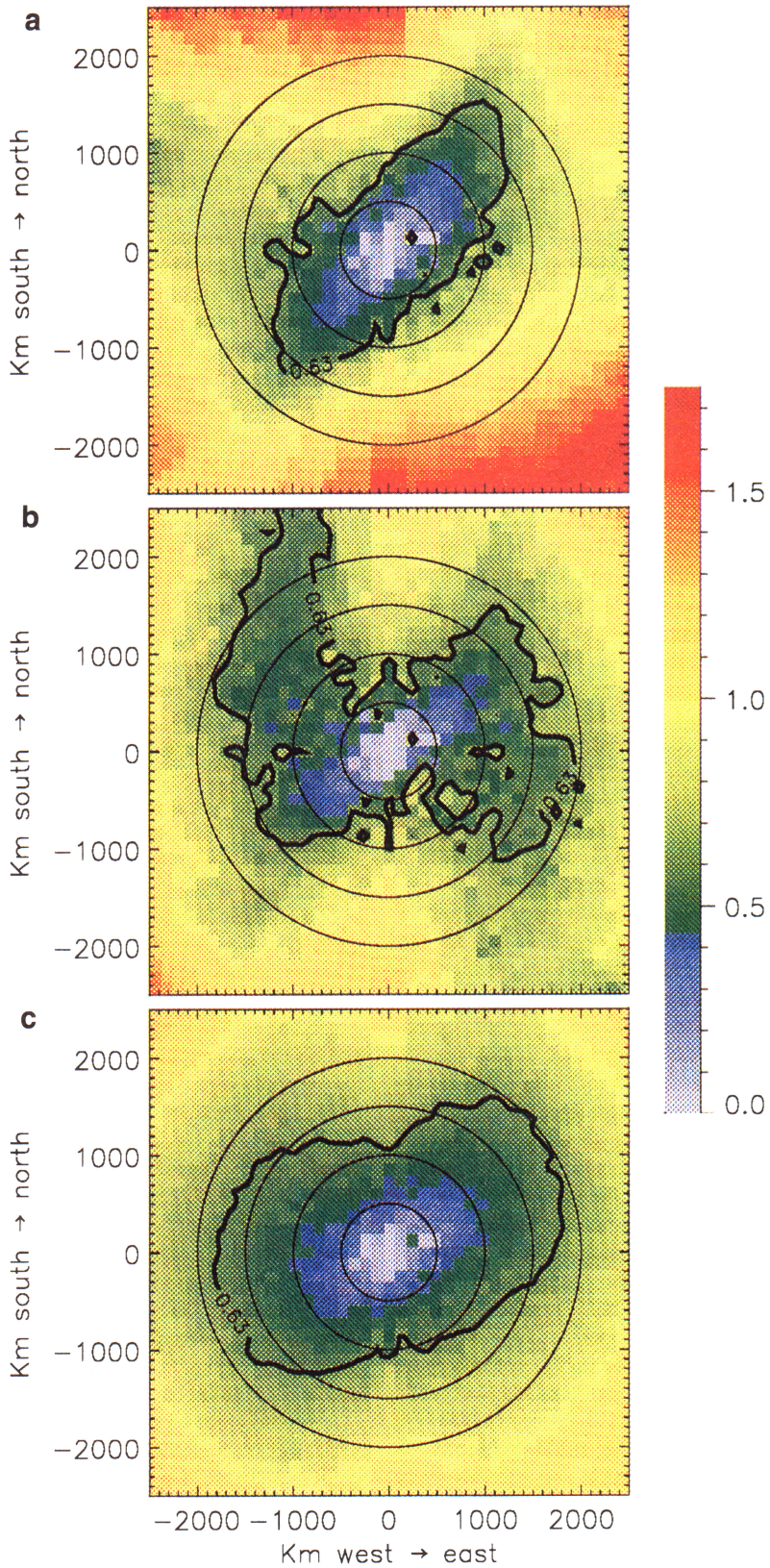

Plate 7. Normalized variograms of sulfate column burden in domain 60°W to 10°W, 30°N to 60°N for (a) October 15, 1986 at 0600 UT. (b) October 22, 1986, at 0600 UT. (c) Average of all variograms for the modeled period. The concentric circles indicate distances from the center in increments of 500 km. The thick line is a contour line for the characteristic value of the variograms, $\gamma = 0.63$.

needed, since the resolution of an Eulerian model is approximately 4 times the horizontal grid spacing [*Pielke,* 1991]. In fact, this variability suggests that the present grid spacing (1.125°) may not be sufficiently fine to completely capture the high spatial variability of the sulfate concentrations and column burdens.

Obviously, the high temporal and spatial variability of the sulfate column burdens cannot be captured by models using low temporal and spatial resolutions. Likewise, this variability will be totally lost in low time-resolution satellite images (weekly or monthly). This lack of proper resolution may be the reason why studies to date have been unable to discern the influence of anthropogenic sulfur on satellite measurements of albedo over the mid North Atlantic, despite the dominance of these sources over biogenic emissions.

5. Summary and Conclusions

We have developed a three-dimensional Eulerian transport and transformation model capable of calculating global sulfate concentrations for actual times and locations and have applied it to calculate sulfate concentrations and column burdens (vertical column integral of the concentration) over the North Atlantic and adjacent continental regions for October 1 to November 15, 1986. Both concentrations and column burdens over the model domain are highly variable and structured in time and space. Vertical distributions are also highly structured, showing frequent instances where concentrations aloft substantially exceed those at ground level. Sulfate concentrations and column burdens at two "snapshot" times: October 15, 1986, at 0600 UT and October 22, 1986, at 0600 UT were directly related to the weather patterns at those times and during the preceding 48 hours.

Source attribution of the sulfate burdens (volume integral of the concentration) for five longitude bands shows that for the time period modeled, anthropogenic sources are the predominant contributors to the sulfate burdens over the middle region of the Atlantic Ocean (20°W to 40°W). North American anthropogenic sources contribute 25 to 58% of the burden to this region, European anthropogenic sources contribute 2% to 33%, mostly south of 35°N and north of 50°N, and biogenic sources contribute 6 to 12%. The significant contribution to the sulfate burden resulting from fluxes from outside the model domain, the need to more accurately represent conditions at the eastern boundary of the domain, and the need to capture episodic aerosol conditions over the Pacific Ocean, lead us to conclude that the model domain must incorporate the entire longitude range for the selected latitude range. The expanded domain should increase the ability of the model to accurately represent sulfate column burdens for specific times and locations, and result in a more complete attribution of the sulfate burdens in the North Atlantic and throughout the hemisphere.

The model also permits attribution of sulfate to formation mechanism: primary, gas phase conversion and aqueous phase conversion. Primary sulfate contributed between 5 and 10% of the sulfate burden resulting from emissions in the model domain, gas phase generated sulfate contributed between 39 and 54%, and aqueous phase generated sulfate contributed between 37 and 55%.

Comparisons of daily average sulfate concentrations at the lowest model level (surface to approximately 65 m) with observations from routine air quality monitoring stations in Europe, Canada, the United States, and Barbados demonstrate that model results closely track the magnitudes, temporal episodicity and absolute magnitudes of the observations. The majority (more than 50%) of model results are within a factor of 3 of the observations. Comparison of the sulfate wet deposition (concentration multiplied by precipitation) with observational data from North American monitoring networks indicates that the majority of model results are within a factor of 3 of the corresponding observations. However, there are problems in the comparisons due to lack of representativeness of the observational data sets. In all but one case, cell averages for the observations were based on a single monitoring station; thus cell-average results from the model are being compared with point observations within the corresponding cell. In addition, most stations are under continental influence and reflect sulfate from proximate anthropogenic sources. Therefore, these comparisons are of restricted utility in assessing the accuracy of long-range features of the model. An additional problem in comparing wet deposition data is that precipitation events at observing stations do not start or end on the 6-hour time resolution of the meteorological data, so discrepancies necessarily occur in aggregation of the modeled data. In general, model results were lower than observations for both sulfate surface concentrations and wet deposition; one source of this underprediction lies in the absence of aqueous phase conversion in nonprecipitating clouds. In addition, sulfate removal is affected by uncertainties in the location and amount of precipitation.

The two major sinks of SO_2 are dry deposition (13 to 17% d^{-1}) and aqueous phase conversion to sulfate (12 to 27% d^{-1}); their relative importance depends on the precipitation encountered. For the domain as a whole, dry deposition is the major sink of SO_2, because anthropogenic emissions are predominantly located east of 30°W, where precipitation during the modeled period was lighter. However, this conclusion is affected by the lack of aqueous phase reactions in nonprecipitating clouds. Turnover times for SO_2 range from 2 to 3 days. Removal of aerosol products (sulfate and MSA) is dominated by wet deposition (9 to 22% d^{-1}), with turnover times ranging from 4 to 8 days, depending on the transport winds and precipitation encountered and on the geographic and vertical distributions. These results are generally comparable with empirical and theoretical estimates of lifetimes of accumulation mode aerosol particles.

The average $1/e$-folding time characterizing the temporal variability of sulfate column burdens in the central North Atlantic (60°W to 10°W; 30°N to 60°N) was 10 hours, with 95% of the values being 25 hours or less, demonstrating that time resolution of less than 24 hours must be used in order to appropriately capture the temporal variability of sulfate fields. The characteristic distance of spatial autocorrelation for this region depends on direction; the minimum value of the average is 900 km and the minimum values of the 10th and 90th percentiles are 400 and 1700 km, demonstrating that the present grid spacing (1.125°) may not be sufficiently fine to capture the high spatial variability of the sulfate concentrations and column burdens.

In conclusion, the three-dimensional Eulerian transport and transformation model for tropospheric sulfate described here appears to be a useful tool for examining sulfate concentrations and burdens on subhemispheric to global scales, pertinent to the issue of radiative forcing of climate by this aerosol. The model employs descriptions of transformation and removal processes similar to those employed in previous models and gives values for turnover times and yields that are consistent with previous estimates obtained with global models. By incorporating fine temporal and spatial resolution similar to that employed in regional-scale models, the model is able to represent the

characteristic variability of sulfate concentrations and column burdens. Use of observation-derived meteorology to drive the model allows sulfate concentrations and column burdens to be compared to observations at specific times and locations. This is quite important in view of the high spatial and temporal variability of these quantities. Comparison of modeled and measured surface concentrations and deposition shows encouraging agreement in the spatial pattern, temporal episodicity, and absolute magnitudes of modeled and observed quantities.

Appendix A: Evaluation of Meteorological Data

The meteorological data used for the present study were part of the ECMWF "first guess" data set, a latitude/longitude transformation of the 6-hour results of the ECMWF spectral forecast model. To compare these data to actual conditions, the following analyses were undertaken. Vector plots of winds were generated at an altitude of 10 m (considered surface winds) and at 500 hPa over North America for October 1 at 1200 UT to November 16 at 1200 UT, and the principal weather features (high- and low-pressure areas, fronts) that were directly identifiable were outlined. Resulting plots were compared with the surface and 500-hPa charts presented in the Daily Weather Summary series [*National Oceanic and Atmospheric Administration (NOAA)*, 1986]. The principal weather features (high- and low-pressure centers, location of fronts) represented in the vector plots compared very well with the corresponding weather depiction in the Daily Weather Summary.

It is specially important that precipitation be accurately described in the transport because wet removal is the primary sink for sulfate aerosol. The ECMWF data include precipitation location and amount; maps were generated showing precipitation location, with differentiation between amounts greater than and less than 0.01 in (0.25 mm, considered trace in the Daily Weather Summary), and compared with the precipitation maps presented in the Daily Weather Summary. The areas covered by the model precipitation above 0.25 mm showed some displacement from the areas covered by the contoured observations, but no consistent patterns were found in the direction of the displacements. However, comparison of the area coverage of trace designation for precipitation amounts showed good agreement between model results and contoured observations.

A more quantitative evaluation of the modeled precipitation fields was attempted using the methodology described by *Anthes et al.* [1989]. Two observational data sets were used for this study; the U.S. Historical Climatology Network Daily Precipitation data set (HCNDP), compiled by the National Climatic Data Center (NCDC) [*Hughes et al.*, 1992] and the daily precipitation data (DPD), also compiled by NCDC, obtained from the National Center for Atmospheric Research (NCAR) [*National Climatic Data Center*, 1990]. The HCNDP data set consists of 136 stations chosen to provide a reasonably homogeneous spatial distribution of stations within the contiguous United States. The DPD data set consists of approximately 700 stations, depending upon the number of valid measurements made on each day of the month. Daily precipitation totals for the observing stations were interpolated on the ECMWF horizontal grid by assigning each of the stations with valid measurements to its nearest node using a distance-weighted space filtering technique described by *Barnes* [1964]. Model daily totals were calculated, and the "bias score" and "categorical forecasts" for the occurrence of a specified precipitation threshold amount were used, with threshold values of 0.25, 2.54 and 6.4 mm. The bias score represents an unpaired comparison; bias scores less than 1 indicate model underprediction. Categorical forecasts compare paired model/observation as a yes/no for the occurrence of the threshold precipitation; results represent the fraction that agree. Bias scores ranged from 0.37 to 0.68 for the HCNDP, and from 0.50 to 0.84 for the DPD data; categorical forecasts ranged from 0.24 to 0.54 for the HCNDP data, and from 0.32 to 0.56 for the DPD data.

These comparisons indicate that the model underpredicts at all threshold values of precipitation relative to observations, with a greater degree of underprediction at the higher thresholds. A large source of uncertainty in these comparisons is the degree of representativeness of the observational data sets. Model results represent averages over the horizontal dimension, whereas observations represent individual points. Thus, average conditions within a model grid cell may not be well represented by the available observations. The higher degree of underprediction by the model at higher thresholds can be highly influenced by insufficient sample of stations within each grid cell and a sample of grid cells that is not large enough to give a reliable bias score. With only one station in a grid cell (this is the case for most of the HCNDP data set), very localized heavy convective rainfall can be reported by the station while the rest of the cell receives a much smaller amount of precipitation. The representativeness problem is further illustrated by the fact that both the bias score and the categorical forecast results had higher favorable scores when the DPD data set was used. In addition, the gridded versions of the two data sets were subjected to paired comparisons; correlation coefficients were 0.66 when all pairs are included, and 0.59 for pairs reporting precipitation greater than zero.

Appendix B: Reaction of DMS with OH

The mechanism for the simplified DMS chemistry used in the present model, derived mainly from the work of *Yin et al.* [1990a, 1990b], is presented schematically in Figure B1, and can be summarized as follows. Atmospheric removal of DMS is initiated by its reaction with OH, NO_3 and $O(^3P)$ radicals. Reactions with $O(^3P)$ and NO_3 are assumed to contribute about 10% of the observed DMS decay and lead to the formation of SO_2. The OH reaction can proceed via addition or via H-atom abstraction. This reaction is represented as

$$CH_3SCH_3 + OH \rightarrow \alpha\ SO_2 + (1\text{-}\alpha)\ MSA$$

where α is the fraction of DMS that converts to SO_2 and $(1-\alpha)$ is the fraction that converts to a nonsulfate aerosol product, which we call MSA. *Hynes et al.* [1986] have derived expressions for the observed rate constant (k) and branching ratios (β_{abs}, fraction of DMS following the abstraction pathway, β_{add} fraction of DMS following the addition pathway) for the OH + CH_3SCH_3 reaction as a function of temperature. The conversion rate of DMS is determined by this initial reaction with OH. End products of DMS oxidation are SO_2 and dimethyl sulfone ($DMSO_2$, $CH_3S(O_2)CH_3$) [*Barnes et al.*, 1988; *Yin et al.*, 1990a, 1990b]. SO_2 can be subsequently oxidized to sulfate or can dry-deposit; $DMSO_2$, being fairly unreactive towards OH and having a high boiling point (511°K), will transfer to the aerosol phase. Further reactions of $DMSO_2$ are not known, but some may lead to the formation of methanesulfonic acid (MSA, CH_3SO_3H); the resulting aerosol species is tracked by the model under the label MSA. Expressions developed by *Hynes et al.* [1986] were used

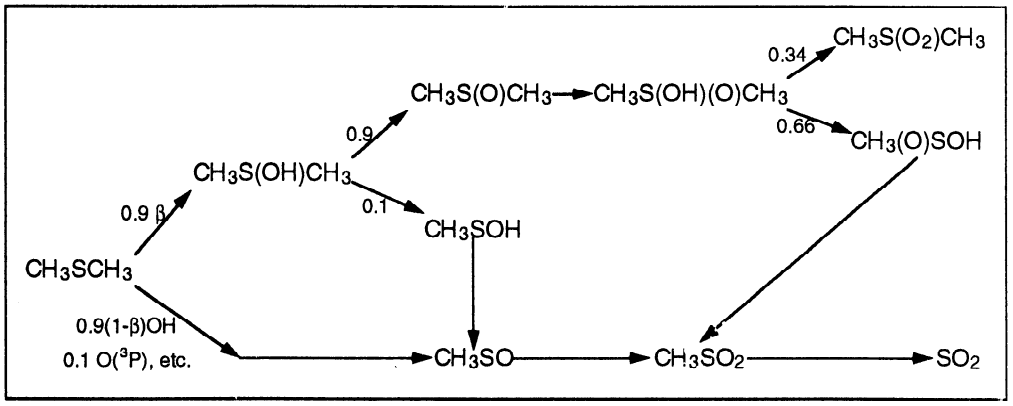

Figure B1. Schematic of the mechanisms for the oxidation of DMS by OH implemented in the model. Here, β is the branching ratio of the addition pathway, and SO_2 yield is the sum of all branches leading to SO_2 production.

to calculate β_{abs}, β_{add}, and the conversion rate of DMS to SO_2 and $DMSO_2$. The yield of SO_2 from OH oxidation of DMS, α, is calculated as the sum of all branches in Figure B1 that lead to SO_2 production.

Table B1 presents the reaction rate constants and yields for the addition and abstraction paths as functions of temperature. Results were calculated using the expressions for k_{obs} and β_{add} derived by *Hynes et al.* [1986]

$$k_{obs} = \frac{Te^{-234/T} + 8.46 \times 10^{-10} e^{7230/T} + 2.68 \times 10^{-10} e^{7810/T}}{1.04 \times 10^{11}\, T + 88.1\, e^{7460/T}}$$

$$k_{abs} = 9.6 \times 10^{-12}\, e^{-234/T} \qquad k_{add} = k_{obs} - k_{abs}$$

$$\beta_{abs} = k_{abs}/k_{obs} \qquad \beta_{add} = 1 - \beta_{abs}$$

where k_{obs} is the observed rate constant, k_{abs} and k_{add} are the rate constants for the abstraction and addition pathways, respectively, and β_{abs} and β_{add} are the branching ratios of the abstraction and addition pathways, respectively.

Table B1. Rate Constants and Branching Ratios for the Reaction of DMS with OH

Temperature, °K	k_{obs}	k_{add}	k_{abs}	β_{add}
240	16.6	13	3.62	0.78
245	16.2	12.5	3.69	0.77
250	15.8	12	3.77	0.76
255	15.2	11.4	3.83	0.75
260	14.5	10.6	3.9	0.73
265	13.6	9.66	3.97	0.71
270	12.5	8.48	4.04	0.68
275	11.2	7.11	4.1	0.63
280	9.82	5.66	4.16	0.58
285	8.51	4.28	4.22	0.5
290	7.38	3.1	4.28	0.42
295	6.52	2.17	4.34	0.33
300	5.89	1.49	4.4	0.25
305	5.47	1.01	4.46	0.19
310	5.2	0.68	4.51	0.13
315	5.03	0.47	4.57	0.09

Here, k_{obs} is the observed rate constant, k_{abs} is the rate constant for abstraction pathway, k_{add} is the rate constant for addition pathway. β_{add} is the branching ratio for addition pathway. k is in 10^{-12} cm^3 s^{-1}.

Acknowledgments. We thank Robert Brown and Victor Casella for assistance in the meteorological analyses, Jane Dignon for supplying the fossil-fuel combustion emissions inventory, Trond Iversen for supplying the EMEP observational network data, Brian Lamb for supplying the programs to generate seasonal gridded values of biogenic land emissions, J. David Mobley for supplying the NAPAP emissions inventory for North America, Joseph Prospero for supplying the observational data for Miami and Barbados, David Simpson for supplying the EMEP emissions inventory for Europe, Robert Vet for supplying the Canadian observational network data, and Judith Williams for typesetting the final manuscript. The meteorological data used were supplied by the European Centre for Medium-Range Weather Forecasts. At Brookhaven National Laboratory this research was performed under the auspices of the U.S. Department of Energy, under contract DE-AC02-76CH00016. Pacific Northwest Laboratory is operated for the Department of Energy by Battelle Memorial Institute under contract DE-AC06-76RLO. C. M. Benkovitz submitted this work in partial fulfillment of the Ph.D. requirements in the Department of Earth System Science at New York University, New York.

References

Anthes, R.A., Y.H. Kuo, E.Y. Hsie, S. Low-Nam, and T.W. Bettge, Estimation of skill and uncertainty in regional numerical models, *Q. J. R. Meteorol. Soc.*, *115*, 763-806, 1989.

Balkanski, Y. J., D.J. Jacob, G.M Gardner, W.C. Graustein, and K.K. Turekian, Transport and residence times of tropospheric aerosols inferred from a global three-dimensional simulation of ^{210}Pb, *J. Geophys. Res.*, *98*, 20,573-20,586, 1993.

Bandy, A.R., D.L. Scott, B.W. Blomquist, S.M. Chen, and D.C. Thornton, Low yields of SO_2 from dimethyl sulfide oxidation in the marine boundary layer, *Geophys. Res. Lett.*, *19*, 1125-1127, 1992.

Barnes, S.L., A technique for maximising details in numerical weather map analysis, *J. Appl. Meteorol.*, *3*, 396-409, 1964.

Barnes, I., V. Bastian, and K.H. Becker, Kinetics and mechanisms of the reaction of OH radicals with dimethyl sulfide, *Int. J. Chem. Kinet.*, *20*, 415-431, 1988.

Bates, T.S., B.K. Lamb, A. Guenther, J. Dignon, and R.E. Stoiber, Sulfur emissions from natural sources, *J. Atmos. Chem.*, *14*, 315-337, 1992.

Benkovitz, C. M., Development and testing of a high-resolution model for tropospheric sulfate driven by observation-derived meteorology, Ph.D. thesis, New York University, New York, 1994.

Berge, E., A regional numerical sulfur dispersion model using a meteorological model with explicit treatment of clouds, *Tellus*, *42B*, 389-407, 1990.

Berkowitz, C.M., R.C. Easter, and B.C. Scott, Theory and results from a quasi-steady-state precipitation-scavenging model, *Atmos. Environ.*, *23*, 1555-1571, 1989.

Berresheim, H., M.O. Andreae, G.P. Ayres, R.W. Gillett, J.T. Merrill, V.J. Davis, and W.L. Chameides, Airborne measurements of dimethylsulfide, sulfur dioxide, and aerosol ions over the Southern Ocean south of Australia, *J. Atmos. Chem.*, *10*, 341-370, 1990.

Bott, A., A positive definite advection scheme obtained by nonlinear renormalization of the advective fluxes, *Mon. Weather Rev.*, *117*, 1006-1015, 1989.

Bridgman, H.A., R.C. Schnell, B.A. Bodhaine, and S.J. Oltmans, Aerosol and ozone distributions over the western North Atlantic during WATOX-86, *Global Biogeochem. Cycles*, *2*, 23-39, 1988.

Cambray, R.S., P.A. Cawse, J.A. Garland, J.A.B. Gibson, P. Johnson, G.N.J. Lewis, D. Newton, L. Salmon, and B.O. Wade, Observations on radioactivity from the Chernobyl accident, *Nucl. Energy*, *26*, 77-101, 1987.

Carmichael, G.R., and L.K. Peters, An Eulerian transport/transformation/removal model for SO_2 and sulfate, I., Model development, *Atmos. Environ.*, *18*, 937-951, 1984a.

Carmichael, G.R., and L.K. Peters, An Eulerian transport/transformation/removal model for SO_2 and sulfate, II., Model calculation of SO_x transport in the eastern United States, *Atmos. Environ.*, *18*, 953-967, 1984b.

Chamberlain, A.C., *Radioactive Aerosols*, Cambridge University Press, New York, 1991.

Chang, J.S., R.A. Brost, I.S.A. Isaksen, S. Madronich, P. Middleton, W.R. Stockwell, and C.J. Walcek, A three-dimensional Eulerian acid deposition model: Physical concepts and formulation, *J. Geophys. Res.*, *92*, 14,681-14,700, 1987.

Charlson, R.J, J. Langner, and H. Rodhe, Sulphate aerosol and climate, *Nature*, *348*, 22, 1990.

Charlson, R.J., J. Langner, H. Rodhe, C.B. Leovy, and S.G. Warren, Perturbation of the northern hemisphere radiative balance by backscattering from anthropogenic aerosols, *Tellus*, *43AB*, 152-163, 1991.

Charlson, R., S.E. Schwartz, J.M. Hales, R.D. Cess, J.A. Coakley, Jr., J.E. Hansen, and D.J. Hoffman, Climate forcing by anthropogenic aerosols, *Science*, *255*, 423-430, 1992.

Daum, P.H., Processes determining cloudwater composition: Inferences from field measurements, in *Acid Deposition at High Elevation Sites*, edited by M.H. Unsworth and D. Fowler, pp. 139-153, Kluwer, Norwell, Mass., 1988.

Dennis, R.L., J.N. McHenry, W.R. Barchet, F.S. Binkowski, and D.W. Byun, Correcting RADM's sulfate underprediction: Discovery and correction of model errors and testing the corrections through comparisons against field data, *Atmos. Environ.*, *27A*, 975-997, 1993.

Deutsch, C.V., and A.G. Journel, *GSLIB Geostatistical Software Library and User's Guide*, Oxford University Press, New York, 1992.

Dietz, R.N., and R.F. Wieser, Sulfate formation in oil-fired power plant plumes. Vol. 1, Parameters affecting primary sulfate emissions and a model for predicting emissions and plume opacity, *Rep. EPRI EA-3231*, Elec. Power Res. Inst., Palo Alto, Calif., 1983.

Dignon, J., NO_x and SO_x emissions from fossil fuels: A global distribution, *Atmos. Environ.*, *26A*, 1157-1163, 1992.

Dignon, J., and S. Hameed, Global emissions of nitrogen and sulfur oxides from 1860 to 1980, *J. Air Pollut. Contr. Assoc.*, *39*, 180-186, 1985.

Durkee, P.A., F. Pfeil, E. Frost, and R. Shema, Global analysis of aerosol particle characteristics, *Atmos. Environ.*, *25A*, 2457-2471, 1991.

Easter, R.C., and D.J. Luecken, A simulation of sulfur wet deposition and its dependence on the inflow of sulfur species to storms, *Atmos. Environ.*, *22*, 2715-2739, 1988.

Easter, R.C., Two modified versions of Bott's positive definite numerical advection scheme, *Mon. Weather Rev.*, *121*, 297-304, 1993.

Eliassen, A., The OECD study of long range transport of air pollutants: Long range transport modelling, *Atmos. Environ.*, *12*, 479-487, 1978.

Eliassen, A., and J. Saltbones, Modelling of long-range transport of sulphur over Europe: A two year model run and some model experiments, *Atmos. Environ.*, *17*, 1457-1473, 1983.

Erickson, R.E., L.M. Yates, R.L. Clark, and D. MacEwen, The reaction of sulfur dioxide with ozone in water and its possible atmospheric significance, *Atmos. Environ.*, *11*, 813-817, 1977.

Erickson, D.J., III, J.J. Walton, S.J. Ghan, and J.E. Penner, Three-dimensional modeling of the global atmospheric sulfur cycle: A first step, *Atmos. Environ.*, *25A*, 2513-2520, 1991.

European Centre for Medium-Range Weather Forecasts, Research Department, ECMWF Forecast model: Adiabatic part, *Rep. Research Manual 2*, Reading, England, 1988.

Falkowski, P.G., Y. Kim, Z. Kolber, C. Wilson, C. Wirick, and R. Cess, Natural versus anthropogenic factors affecting low-level cloud albedo over the North Atlantic, *Science*, *256*, 1311-1313, 1992.

Ferek, R.J., D.A. Hegg, J.A. Herring, and P.V. Hobbs, An improved filter pack technique for airborne measurement of low concentrations of SO_2, *J. Geophys. Res.*, *96*, 22,373-22,378, 1991.

Forgan, B.W., Aerosol optical depth, in *Baseline Atmospheric Program (Australia) 1985*, edited by B.W. Forgan and P.J. Fraser, pp. 50-56, Department of Science/Bureau of Meteorology and Commonwealth Scientific and Industrial Research Organization/Division of Atmospheric Research, Australia, 1987.

Galloway, J.N., *et al.*, Sulfur and nitrogen levels in the North Atlantic Ocean's atmosphere: A synthesis of field and modeling results, *Global Biogeochem. Cycles*, *6*, 77-100, 1992.

Giorgi, F., and W.L. Chameides, Rainout lifetimes of highly soluble aerosols and gases as inferred from simulations with a general circulation model, *J. Geophys. Res.*, *91*, 14,367-14,376, 1986.

Han, Q., W.B. Rossow, and A.A. Lacis, Near-global survey of effective droplet radii in liquid water clouds using ISSCP data, *J. Clim.*, *7*, 465-497, 1994.

Hass, H., H.J. Jakobs, M. Memmesheimer, A. Ebel, and J.S. Chang, Simulation of a wet deposition case in Europe using the European acid deposition model (EURAD), in *Air Pollution Modeling and Its Application VIII*, edited by H. van Dop and D.G. Steyn, pp. 205-213, Plenum, New York, 1991.

Hesstvedt, E., Ø. Hov, and I.S.A. Isaksen, Quasi-steady-state approximations in air pollution modeling: Comparison of two numerical schemes for oxidant prediction, *Int. J. Chem. Kinet.*, *10*, 971-994, 1978.

Hofmann, D.J., Increase in the stratospheric background sulfuric acid aerosol mass in the past 10 years, *Science*, *248*, 996-1000, 1990.

Hughes, P.Y., E.H. Mason, T.R. Karl, and W.A. Brower, United States historical climatology network daily temperature and precipitation data, *Rep. ORNL/CDIAC-50. NDP042*, Carbon Dioxide Inf. Anal. Cent., Oak Ridge Natl. Lab., Oak Ridge, Tenn., 1992.

Husain, L., and V.A. Dutkiewicz, A long-term (1975-1988) study of atmospheric SO_4^{2-}: Regional contributions and concentration trends, *Atmos. Environ.*, *24A*, 1175-1187, 1990.

Hynes, A.J., P.H. Wine, and D.H. Semmes, Kinetics and mechanisms of OH reactions with organic sulfides, *J. Phys. Chem.*, *90*, 4148-4156, 1986.

Isaaks, E.H., and R.M. Srivastava, *An Introduction to Applied Geostatistics*, Oxford University Press, New York, NY, 1989.

Iversen, T., N.E. Halvorsen, J. Saltbones, and H. Sandnes, Calculated budgets for airborne sulphur and nitrogen in Europe, *Rep. EMEP/MSC-W 1/91*, Meteorol. Synthesizing Cent. West, Norw. Meteorol. Inst., Oslo, 1990.

Junge, C.E., *Air Chemistry and Radioactivity*, Academic, New York, 1963.

Kiehl, J.T., and B.P. Briegleb, The relative roles of sulfate aerosols and greenhouse gases in climate forcing, *Science*, *260*, 311-314, 1993.

Kim, Y., and R.D. Cess, Effect of anthropogenic sulfate aerosols on low-level cloud albedo over oceans, *J. Geophys. Res.*, *98*, 14,883-14,885, 1993.

Langner, J., and H. Rodhe, A global three-dimensional model of the tropospheric sulfur cycle, *J. Atmos. Chem.*, *13*, 225-263, 1991.

Langner, J., *et al.*, The global atmospheric sulfur cycle: An evaluation of model predictions and observations, *Rep. CM-81*, Dep. of Meteorol., Stockholm Univ., Int. Meteorol. Inst. in Stockholm, 1993.

Lipfert, F.W., Filter artifacts associated with particulate measurements: New evidence and effects on statistical relationships, *Atmos. Environ.*, *in press*, 1994.

Logan, J.A., M.J. Prather, S.C. Wofsy, and M.B. McElroy, Tropospheric

chemistry: A global perspective, *J. Geophys. Res.*, *86*, 7210-7254, 1981.

Louis, J.-F, A parameteric model of vertical eddy fluxes in the atmosphere, *Boundary Layer Meterol.*, *17*, 187-202, 1979.

Luecken, D.J., C.M. Berkowitz, and R.C. Easter, Use of a three-dimensional cloud-chemistry model to study the transatlantic transport of soluble sulfur species, *J. Geophys. Res.*, *96*, 22,477-22,490, 1991.

Matthews, E., Atlas of archived vegetation, land-use and seasonal albedo data sets, *NASA Tech. Memo. 86199*, 1985.

Modica, L.G., and D.R. Dulleba, The 1985 NAPAP emissions inventory: Development of spatial allocation factors, *Rep. EPA-600/7-89-010b*, U.S. Environ. Prot. Agency, Research Triangle Park, N. C., 1990.

NASA, Chemical kinetics and photochemical data for use in stratospheric modeling, *JPL Publ. 85-37*, 1991.

National Climatic Data Center, Hourly precipitation data, *Rep. TD-3240*, Natl. Oceanic and Atmos. Admin., Washington, D. C., 1990.

National Oceanic and Atmospheric Administration, Daily weather maps, Washington, D. C., 1986.

Pasquill, F., The dispersion of material in the atmospheric boundary layer - The basis for generalization, in *Lectures on Air Pollution and Environmental Impact Analyses*, edited by D.A. Haugen, pp. 1-34, American Meteorological Society, Boston, Mass., 1976.

Pielke, R.A., A recommended specific definition of "resolution", *Bull. Am. Meterol. Soc.*, *72*, 1912, 1991.

Rodhe, H., and I. Isaksen, Global distribution of sulfur compounds in the troposphere estimated in a height/latitude transport model, *J. Geophys. Res.*, *85*, 7401-7409, 1980.

Saeger, M., *et al.*, The 1985 NAPAP emissions inventory (version 2): Development of the annual data and modelers' tapes, *Rep. EPA-600/7-89-012a*, U.S. Environ. Prot. Agency, Research Triangle Park, N. C., 1989.

Schaug, J., J.E. Skjelmoen, S.E. Walker, A. Harstad, K. Nodop, and J. Pacyna, Data report 1986. Part I: Annual summaries, *EMEP-CCC-Rep. 6/88, Reference O-7727*, Norw. Inst. for Air Res., Lillestrøm, 1988.

Schaug, J., J.E. Skjelmoen, S.E. Walker, U. Pedersen, and A. Harstad, Data report 1987. Part 1: Annual summaries, *EMEP/CCC Rep. 1/89, Reference O-7727*, Norw. Inst. for Air Res., Lillestrøm, 1989.

Schwartz, S.E., Residence times in reservoirs under non-steady state conditions: Application to atmospheric SO_2 and aerosol sulfate, *Tellus*, *31*, 530-547, 1979.

Schwartz, S.E., Are global cloud albedo and climate controlled by marine phytoplankton?, *Nature*, *336*, 441-445, 1988a.

Schwartz, S.E., Mass-transport limitation to the rate of in-cloud oxidation of SO_2: Re-examination in the light of new data, *Atmos. Environ.*, *22*, 2491-2499, 1988b.

Sedlacek, W.A., E.J. Mroz, A.L. Lazrus, and B.W. Gandrud, A decade of stratospheric sulfate measurements compared with observations of volcanic eruptions, *J. Geophys. Res.*, *88*, 3741-3776, 1983.

Shea, D.J., *Climatological Atlas: 1950-1979*, National Center for Atmospheric Research, Boulder, Colo., 1986.

Sheih, C.M., M.L. Wesely, and C.J. Walcek, A dry deposition module for regional acid deposition, *Rep. EPA/600/3-86/037*, U.S. Environ. Prot. Agency, Research Triangle Park, N. C., 1986.

Simmons, A.J., and R. Struffing, An energy and angular-momentum conserving finite difference scheme, hybrid coordinates and medium-range weather prediction, *Tech. Rep. 28*, Eur. Cent. for Medium-Range Weather Forecasts, Reading, England, 1981.

Sirois, A., and L.A. Barrie, An estimate of the importance of dry deposition as a pathway of acidic substances from the atmosphere to the biosphere in eastern Canada, *Tellus*, *40B*, 59-80, 1988.

Slinn, W.G.N., Air-to-sea transfer of particles, in *Air-to-Sea Exchange of Gases and Particles*, edited by P.S. Liss and W.G.N. Slinn, pp. 299-405, D. Reidel, Hingham, Mass, 1983.

Spiro, P.A., D.J. Jacob, and J.A. Logan, Global inventory of sulfur emissions with a 1° x 1° resolution, *J. Geophys. Res.*, *97*, 6023-6036, 1992.

Spivakovsky, C.M., R. Yevich, J.A. Logan, S.C. Wofsy, M.B. McElroy, and M.J. Prather, Tropospheric OH in a three-dimensional chemical tracer model: An assessment based on observations of CH_3CCl_3, *J. Geophys. Res.*, *95*, 18,441-18,471, 1990.

Tarrason, L., and T. Iversen, The influence of North American anthropogenic sulphur emissions over western Europe, *Tellus*, *44B*, 114-132, 1992.

ten Brink, H.M., S.E. Schwartz, and P.H. Daum, Efficient scavenging of aerosol sulfate by liquid-water clouds, *Atmos. Environ.*, *21*, 2035-2052, 1987.

Trenberth, K.E, and J.G. Olson, Evaluation of NMC global analyses: 1979-1987, *Rep. NCAR/TN-299+STR*, Natl. Cent. for Atmos. Res., Boulder, Colo., 1988.

Trenberth, K.E., Climate diagnostics from global analyses: Conservation of mass in ECMWF analyses, *J. Clim.* *4*, 707-722, 1991.

Twomey, S.A., *Atmospheric Aerosols*, Elsevier, New York, 1977.

Twomey, S.A., M. Piepgrass, and T.L. Wolfe, An assessment of the impact of pollution on global cloud albedo, *Tellus*, *36B*, 356-366, 1984.

U.S. Environmental Protection Agency, *AIRS User's Guide*, Office of Air Quality Planning and Standards, Research Triangle Park, N. C., 1988.

Venkatram, A., and P. Karamchandani, Source receptor relationships: A look at acid deposition modeling, *Environ. Sci. Technol.*, *20*, 1084-1091, 1986.

Voldner, E.C., L.A. Barrie, and A. Sirois, A literature survey of dry deposition of oxides of sulfur and nitrogen with emphasis on long-range transport modelling in north america, *Atmos. Environ.*, *20*, 2101-2123, 1986.

Walcek, C.J., and G.R. Taylor, A theoretical method for computing vertical distributions of acidity and sulfate production within cumulus clouds, *J. Atmos. Sci.*, *43*, 339-355, 1986.

Walton, J.J., M.C. MacCracken, and S.J. Ghan, A global-scale lagrangian trace species model of transport, transformation and removal processes, *J. Geophys. Res.*, *93*, 8339-8354, 1988.

Warner, J., On steady state one-dimensional models of cumulus convection, *J. Atmos. Sci.*, *27*, 1035-1040, 1970.

Watson, C.R., and A.R. Olsen, Acid deposition system (ADS) for statistical reporting: System design and user's code manual, *Rep. EPA-600/8-84-023*, U.S. Environ. Prot. Agency, Research Triangle Park, N. C., 1984.

Wesely, M., Simplified techniques to study components of solar radiation under haze and clouds, *J. Appl. Meteorol.*, *21*, 373-383, 1982.

Wesely, M., Parameterization of surface resistances to gaseous dry deposition in regional-scale numerical models, *Atmos. Environ.*, *23*, 1293-1304, 1989.

Wigley, T.M.L., and S.C.B. Raper, Implications for climate and sea level of revised IPCC emissions scenarios, *Nature*, *357*, 293-300, 1992.

Williams, R.M., A model for the dry deposition of particles to natural water surfaces, *Atmos. Environ.*, *16*, 1933-1938, 1982.

Wilson, M.F., and A. Henderson-Sellers, A global archive of land cover and soils data for use in general circulation models, *J. Clim.*, *5*, 119-143, 1985.

Yanenko, N.N., *The Method of Fractional Steps*, Springer, Berlin, 1971.

Yin, F., D. Grosjean, and J.H. Seinfeld, Photooxidation of dimethyl sulfide and dimethyl disulfide, I, Mechanism development, *J. Atmos. Chem.*, *11*, 309-364, 1990a.

Yin, F., D. Grosjean, R.C. Flagan, and J.H. Seinfeld, Photooxidation of dimethyl sulfide and dimethyl disulfide, II, Mechanism evaluation, *J. Atmos. Chem.*, *11*, 365-399, 1990b.

Zimmerman, R.R., Testing for hydrocarbon emissions from vegetation leaf litter and aquatic surfaces, and development of a methodology for compiling biogenic emissions inventories, U.S. Environ. Prot. Agency, Research Triangle Park, N. C., 1979.

C. M. Benkovitz, S. Nemesure, S. E. Schwartz, and R. Wagener, Brookhaven National Laboratory, Upton, NY 11973. (e-mail: cmb@bnl.gov; seth@gown.das.bnl.gov; ses@bnl.gov; wagener@bnl.gov).

C. M. Berkowitz and R. C. Easter, Pacific Northwest Laboratory, Richland, WA 99352. (e-mail: cm_berkowitz@pnl.gov; rc_easter@pnl.gov).

(Received January 24, 1994; revised June 13, 1994; accepted June 17, 1994.)